Downlink Single-Snapshot Localization and Mapping with a Single-Antenna Receiver

Citation for the original published paper (version of record):

N.B. When citing this work, cite the original published paper.

(article starts on next page)

Downlink Single-Snapshot Localization and Mapping with a Single-Antenna Receiver

Alessio Fascista, *Member, IEEE*, Angelo Coluccia, *Senior Member, IEEE*, Henk Wymeersch, *Senior Member, IEEE*, and Gonzalo Seco-Granados, *Senior Member, IEEE*

Abstract—5G mmWave MIMO systems enable accurate estimation of the user position and mapping of the radio environment using a single snapshot when both the base station (BS) and user are equipped with large antenna arrays. However, massive arrays are initially expected only at the BS side, likely leaving users with one or very few antennas. In this paper, we propose a novel method for single-snapshot localization and mapping in the more challenging case of a user equipped with a single-antenna receiver. The joint maximum likelihood (ML) estimation problem is formulated and its solution formally derived. To avoid the burden of a full-dimensional search over the space of the unknown parameters, we present a novel practical approach that exploits the sparsity of mmWave channels to compute an approximate joint ML estimate. A thorough analysis, including the derivation of the Cramér-Rao lower bounds, reveals that accurate localization and mapping can be achieved also in a MISO setup even when the direct line-of-sight path between the BS and the user is severely attenuated.

Index Terms—mmWave, localization, mapping, MIMO, multiple-input single-output (MISO), 5G cellular networks, AOD, SLAM

I. INTRODUCTION

THE advent of fifth-generation (5G) mobile cellular communications is paving the way for a technological revolution [1], [2]. Millimeter wave (mmWave) signals and massive multiple-input multiple-output (MIMO) technologies are regarded as key pillars of emerging 5G systems, thanks to the expected high data rates and spectral efficiency [3]–[5]. Large bandwidths and massive antenna arrays make also possible very precise estimation of location-related information such as time-of-flight (TOF), angle-of-arrival (AOA), and angle-of-departure (AOD), which can enable applications requiring accurate localization [6]–[8].

The localization capabilities of mmWave MIMO systems have received significant attention. In [9] the Cramér-Rao Lower bound (CRLB) for the problem of 3D localization is derived, highlighting the main differences in the achievable accuracy between uplink (UL) and downlink (DL) channels.

A. Fascista and A. Coluccia are with the Department of Innovation Engineering, Università del Salento, Via Monteroni, 73100 Lecce, Italy (e-mail: alessio.fascista@unisalento.it; angelo.coluccia@unisalento.it).

H. Wymeersch is with the Department of Electrical Engineering, Chalmers University of Technology, 412 96 Gothenburg, Sweden (e-mail: henkw@chalmers.se).

G. Seco-Granados is with the Department of Telecommunications and Systems Engineering, Universitat Autònoma de Barcelona, 08193 Barcelona, Spain (e-mail: gonzalo.seco@uab.cat).

The theoretical analysis revealed that mmWave MIMO systems can provide cm-level accuracy even when the positioning process is supported by a single base station (BS). Over the last years, a number of localization algorithms have appeared in the literature [10]–[13].

Differently from conventional radio-frequency systems, the peculiar characteristics of mmWave MIMO channels make it possible to estimate position-related parameters for each received non-line-of-sight (NLOS) path [14]; remarkably, the Fisher information analysis in [15] demonstrated that NLOS components provide additional information over the line-of-sight (LOS) path, which can be fruitfully leveraged to improve the localization performance. In addition to accurately localizing one or more users, mmWave MIMO can be also exploited to progressively build a map of the radio environment over time, a problem that can be categorized as a simultaneous localization and mapping (SLAM) problem (for more details on the topic, please refer to [16], [17]). A few papers have recently started to address this problem, specifically to exploit NLOS paths for both position estimation and mapping in mmWave MIMO [18]–[21]. Thanks to the high temporal and spatial resolution, the TOFs, AOAs and AODs originating from multipath propagation can be directly linked to the positions of BSs, users, and physical scatterers or reflectors at each time instant, allowing the SLAM problem to be solved using only a single snapshot of the environment.

While mmWave MIMO enables high positioning and mapping accuracy with a single snapshot, it requires the deployment of large-scale antenna arrays at the user side, considerably increasing the complexity and cost of the overall system. In contrast, mobile users using smartphones, as well as wearable/portable IoT devices, will be initially equipped with one or very few antennas [22]. Localization and mapping using a single antenna at both transmit and receive side, namely single-input single-output (SISO), has been addressed in the context of ultrawide-band systems. Differently from the MIMO case, only TOF or RSS information can be used in the estimation process, which in turn requires multiple snapshots corresponding to different positions of the user to lead to an identifiable SLAM solution [23], [24]. A recently-introduced alternative consists in adopting the emerging technology of reconfigurable intelligent surfaces (RISs), whose advantage is that the reflection angle of the NLOS path impinging on it can be modified by the transmitter, so injecting a degree of control in the physical propagation environment. This technology indeed opens the doors to unprecedented opportunities, but it will take even longer to have it widespread in commercial

systems [25]–[27].

Aimed at partially closing the knowledge gap between MIMO and SISO systems, in this paper we investigate the challenging problem of single-snapshot localization and mapping in the forthcoming multiple-input single-output (MISO) case of a mmWave system, i.e., the user is equipped with a single-antenna receiver while the BS has a transmit array. Specifically, we exploit the TOF and AOD information associated to the DL signals transmitted from a single BS, allowing single-snapshot localization and mapping, even in the presence of NLOS paths. The use of DL as opposed to UL signals leads to better signal-to-noise ratio (SNR) conditions for the estimation problem [28]. Although the MISO setup may appear as a mere simplified version of the MIMO case, there are fundamental differences that should be carefully taken into account when facing the SLAM problem. First, MISO channels are characterized by fewer position-related measurements per path (only AODs and TOFs), being the MS unable to estimate the AOAs of the impinging signals. One the one hand, this directly affects the fundamental identifiability of the SLAM problem, as it will be discussed in Sec. III-D. On the other hand, from an algorithmic perspective the lack of AOAs information does not allow a direct application of the same estimation approaches used in the MIMO case, where both the angular dimensions (AODs and AOAs) are jointly exploited for channel estimation. The main contributions of this work are as follows:

- *A fundamental Fisher information analysis* is conducted, which allows to understand the problem from a theoretical perspective, extending the CRLB analysis for the LOS-only scenario in [29] with a thorough evaluation of the achievable performance when the NLOS paths are explicitly taken into account in the estimation process. Remarkably, we will show that accurate single-snapshot localization and mapping is still possible in a MISO setup, but in contrast to the MIMO case, map information does not increase the user position information;
- *The derivation of the maximum likelihood (ML) estimator for localization and mapping* is provided, showing the equivalence of channel-domain and position-domain formulations. Furthermore, we show that mapping of the scatterers positions depends also on the estimation accuracy of LOS parameters, in line with the Fisher information analysis.
- *A low-complexity estimator* is proposed, by exploiting the sparsity of the mmWave channel. We design an efficient two-step algorithm which allows the computation of an accurate approximate solution of the joint ML estimation problem, but avoiding the need of a full-dimensional search in the space of the unknown parameters.

A thorough simulation analysis demonstrates that the proposed joint ML algorithm enables a very accurate estimation of the user position and mapping of the scatterers locations, with performances attaining the theoretical lower bounds even when the LOS path is severely attenuated.

The rest of the paper is organized as follows. In Sec. II, we introduce the system model and describe in details the reference scenario. In Sec. III, we derive and analyze the fundamental bounds on the estimation of the channel and location parameters in the considered MISO setup. Then, in Sec. IV we formulate the joint ML estimation problem in the channel domain and propose a novel low-complexity localization and mapping approach; furthermore, we discuss the equivalence with the joint ML estimator in the position domain. The performance of the proposed approach is then assessed in Sec. V. We conclude the paper in Sec. VI.

II. SYSTEM MODEL

The reference scenario addressed in this paper consists of a MISO system in which a BS, equipped with N_{BS} antennas, communicates with a mobile station (MS) equipped with a single antenna receiver. The system operates at a carrier frequency f_c (corresponding to wavelength λ_c) and uses signals having bandwidth B. Without loss of generality, the BS is located in the origin, i.e., $\boldsymbol{p}_{\text{BS}} = [0\ 0]^{\text{T}}$, while we denote by $\boldsymbol{p} = [p_x\ p_y]^{\text{T}}$ the unknown position of the MS.

A. Transmitter Model

We consider the transmission of orthogonal frequency division multiplexing (OFDM) signals. Particularly, we assume that G signals are broadcast in DL sequentially, with the g-th transmission consisting in M simultaneously transmitted symbols over each subcarrier $n = 0, \ldots, N-1$, i.e., $\boldsymbol{x}^g[n] = [x_1[n]\ \cdots\ x_M[n]]^{\text{T}} \in \mathbb{C}^{M \times 1}$, with $P_t = \mathbb{E}\left[\|\boldsymbol{x}^g[n]\|^2\right]$ the transmitted power and $\mathbb{E}[\cdot]$ denoting the expectation operator. After precoding, the symbols are transformed to the time-domain using an N-point Inverse Fast Fourier Transform (IFFT). A cyclic prefix (CP) of length $T_{\text{CP}} = DT_S$ is added before the radio-frequency (RF) precoding, with D number of symbols in the CP and $T_S = 1/B$ the sampling period.

The signal transmitted over subcarrier n at time g is expressed as $\boldsymbol{z}^g[n] = \boldsymbol{F}^g[n]\boldsymbol{x}^g[n]$, with $\boldsymbol{F}^g[n] \in \mathbb{C}^{N_{\text{BS}} \times M}$ denoting the hybrid analog/digital beamforming matrix applied at the transmit side. Specifically, assuming the availability of N_{RF} RF chains at the BS, we can denote $\boldsymbol{F}^g[n] = \boldsymbol{F}_{\text{RF}}\boldsymbol{F}_{\text{BB}}^g[n]$ where $\boldsymbol{F}_{\text{RF}} \in \mathbb{C}^{N_{\text{BS}} \times N_{\text{RF}}}$ is the analog RF precoder while $\boldsymbol{F}_{\text{BB}}^g[n] \in \mathbb{C}^{N_{\text{RF}} \times M}$ is the digital (baseband) precoder [30], [31]. In absence of a priori knowledge about the user location, the M beams in the beamforming matrix are typically set to ensure a uniform coverage of the considered area. Furthermore, a total power constraint $\|\boldsymbol{F}^g[n]\|_{\text{F}} = 1$ is imposed to the transmit beamforming [32]. Given the typical sparsity of the mmWave channels, less beams than antenna elements can be considered, i.e., $M \leq N_{\text{BS}}$ [33], [34].

B. Channel Model

We assume that a direct LOS link exists between the BS and the MS, and that additional NLOS paths due to local scatterers or reflectors may also be present. Since we are dealing with a single-snapshot localization and mapping problem assuming far-field propagation, the difference between the reflective characteristics of scatterers and reflectors (with large flat surfaces) can be neglected; notice however that such aspects
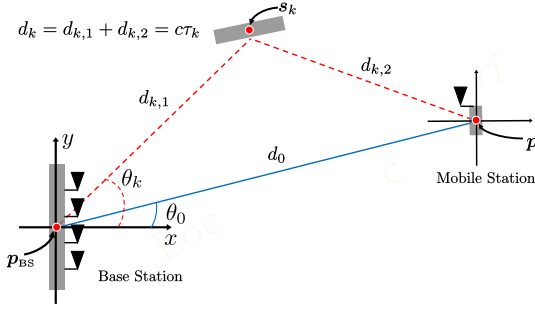
Fig. 1: Geometry of the considered two-dimensional localization and mapping scenario.

should be taken into account when moving towards multi-snapshot or near-field localization. For the sake of the analysis, we also assume that the system has been synchronized during an initial phase using, e.g., a two-way protocol [35], [36]. The different position-related parameters of the channel are depicted in Fig. 1. These parameters include θ_k and τ_k, denoting the AOD and TOF related to the k-th path, respectively. In the following, $k = 0$ corresponds to the LOS link and $k \geq 1$ denotes the NLOS paths. Moreover, we denote by $\boldsymbol{s}_k = [s_{k,x} \ s_{k,y}]^{\text{T}}$ the unknown position of the scatterer giving rise to k-th NLOS path, for which $d_{k,1} = \|\boldsymbol{s}_k - \boldsymbol{p}_{\text{BS}}\| = \|\boldsymbol{s}_k\|$ and $d_{k,2} = \|\boldsymbol{p} - \boldsymbol{s}_k\|$, with $\|\cdot\|$ denoting the Euclidean distance. We consider by convention $\boldsymbol{s}_0 \equiv \boldsymbol{p}$, making all expressions well-defined also for $k = 0$. Assuming $K+1$ paths, the $1 \times N_{\text{BS}}$ channel vector associated with subcarrier n is given by

$$\boldsymbol{h}^{\text{T}}[n] = \boldsymbol{\zeta}^{\text{T}}[n]\boldsymbol{A}_{\text{BS}}^{\text{H}} \tag{1}$$

where we leveraged $\lambda_n = c/(\frac{n}{NT_S} + f_c) \approx \lambda_c \ \forall n$ (with c denoting the speed of light), i.e., the typical narrowband condition. The array response matrix is given by

$$\boldsymbol{A}_{\text{BS}} = [\boldsymbol{a}_{\text{BS}}(\theta_0), \dots, \boldsymbol{a}_{\text{BS}}(\theta_K)] \tag{2}$$

and $[\boldsymbol{\zeta}[n]]_k = \sqrt{N_{\text{BS}}}\alpha_k \text{e}^{\frac{-j2\pi n\tau_k}{NT_S}}$, with $\alpha_k = h_k/\sqrt{\rho}_k$, with ρ_k the path loss and h_k denoting the complex channel gain of the k-th path, respectively. Without loss of generality, in the following we consider a Uniform Linear Array (ULA) without mutual antenna coupling and with isotropic antennas, whose steering vector can be expressed as $\boldsymbol{a}_{\text{BS}}(\theta) = \frac{1}{\sqrt{N_{\text{BS}}}}\left[1 \ e^{j\frac{2\pi}{\lambda_c}d\sin\theta} \ \cdots \ e^{j(N_{\text{BS}}-1)\frac{2\pi}{\lambda_c}d\sin\theta}\right]^{\text{T}}$ where $d = \frac{\lambda_c}{2}$ denotes the ULA interelement spacing.

C. Received Signal Model

The received signal related to the n-th subcarrier and transmission g, after CP removal and Fast Fourier Transform (FFT), is given by

$$y^g[n] = \boldsymbol{h}^{\text{T}}[n]\boldsymbol{F}^g[n]\boldsymbol{x}^g[n] + \nu^g[n] \tag{3}$$

where $\nu^g[n]$ is the additive circularly complex Gaussian noise with zero mean and variance σ^2. The objective of the paper is to determine the unknown MS position $\boldsymbol{p}$ as well as to map the

location of the scatterers $\boldsymbol{s}_k$, $k \geq 1$ present in the environment from the set of all received signals

$$\boldsymbol{Y} = \begin{bmatrix} y^1[0] & \cdots & y^G[0] \\ \vdots & \ddots & \vdots \\ y^1[N-1] & \cdots & y^G[N-1] \end{bmatrix}. \tag{4}$$

III. MISO: FUNDAMENTAL BOUNDS IN MULTIPATH SCENARIO

In this section, we aim to gain a fundamental understanding of the MISO localization and mapping problem, in particular in terms of identifiability, the role of the NLOS paths. To this end, we apply the framework of Fisher information theory [37], which has been widely used in the context of localization [38]. In particular, we derive the analytical expressions of the Fisher Information Matrix (FIM) and its inverse, related to the estimation of the MS position $\boldsymbol{p}$ and scatterers positions $\boldsymbol{s}_k$. As a first step, we evaluate the theoretical bounds on the estimation of the channel parameters (i.e., AODs, TOFs, and channel gains). Subsequently, such bounds are transformed in the position domain and further analyzed to gain insights on the achievable performance in terms of joint localization of the user and mapping of the environment. We will show that, in contrast to a MIMO setup, NLOS paths with unknown origin can only degrade the localization performance of the MS.

A. FIM on Channel Parameters

Let $\boldsymbol{\gamma} \in \mathbb{R}^{4(K+1)\times 1}$ denotes the vector of the unknown channel parameters $\boldsymbol{\gamma} = [\boldsymbol{\gamma}_0^{\text{T}} \cdots \boldsymbol{\gamma}_K^{\text{T}}]^{\text{T}}$, where each $\boldsymbol{\gamma}_k$ consists of the channel complex amplitude, TOF and AOD for the k-th path and is given by $\boldsymbol{\gamma}_k = [r_k \ \phi_k \ \tau_k \ \theta_k]^{\text{T}}$, with r_k and ϕ_k modulus and phase of the complex amplitude $\alpha_k = h_k/\sqrt{\rho}_k \overset{\text{def}}{=} r_k e^{j\phi_k}$, respectively. Defining $\hat{\boldsymbol{\gamma}}$ as an unbiased estimator of $\boldsymbol{\gamma}$, the mean squared error (MSE) is lower bounded as

$$\mathbb{E}_{\boldsymbol{Y}|\boldsymbol{\gamma}}\left[(\hat{\boldsymbol{\gamma}} - \boldsymbol{\gamma})(\hat{\boldsymbol{\gamma}} - \boldsymbol{\gamma})^{\text{T}}\right] \succeq \boldsymbol{J}_{\boldsymbol{\gamma}}^{-1} \tag{5}$$

where $\mathbb{E}_{\boldsymbol{Y}|\boldsymbol{\gamma}}[\cdot]$ denotes the expectation parameterized as function of the unknown vector $\boldsymbol{\gamma}$ and $\boldsymbol{J}_{\boldsymbol{\gamma}}$ is the $4(K+1)\times 4(K+1)$ FIM defined as $\boldsymbol{J}_{\boldsymbol{\gamma}} = \mathbb{E}_{\boldsymbol{Y}|\boldsymbol{\gamma}}\left[-\frac{\partial^2 \log f(\boldsymbol{Y}|\boldsymbol{\gamma})}{\partial\boldsymbol{\gamma}\partial\boldsymbol{\gamma}^{\text{T}}}\right]$. Notice that the existence of $\boldsymbol{J}_{\boldsymbol{\gamma}}^{-1}$ only requires that certain regularity conditions are satisfied [37]. The FIM can be structured as

$$\boldsymbol{J}_{\boldsymbol{\gamma}} = \begin{bmatrix} \boldsymbol{\Lambda}(\boldsymbol{\gamma}_0, \boldsymbol{\gamma}_0) & \cdots & \boldsymbol{\Lambda}(\boldsymbol{\gamma}_0, \boldsymbol{\gamma}_K) \\ \vdots & \ddots & \vdots \\ \boldsymbol{\Lambda}(\boldsymbol{\gamma}_K, \boldsymbol{\gamma}_0) & \cdots & \boldsymbol{\Lambda}(\boldsymbol{\gamma}_K, \boldsymbol{\gamma}_K) \end{bmatrix} \tag{6}$$

where the 4×4 matrix $\boldsymbol{\Lambda}(\boldsymbol{\gamma}_h, \boldsymbol{\gamma}_\ell)$ is given by

$$\boldsymbol{\Lambda}(\boldsymbol{\gamma}_h, \boldsymbol{\gamma}_\ell) = \mathbb{E}_{\boldsymbol{Y}|\boldsymbol{\gamma}}\left[-\frac{\partial^2 \log f(\boldsymbol{Y}|\boldsymbol{\gamma})}{\partial\boldsymbol{\gamma}_h\partial\boldsymbol{\gamma}_\ell^{\text{T}}}\right]$$

$$= \begin{bmatrix} \Lambda(r_h, r_\ell) & \Lambda(r_h, \phi_\ell) & \Lambda(r_h, \tau_\ell) & \Lambda(r_h, \theta_\ell) \\ \Lambda(\phi_h, r_\ell) & \Lambda(\phi_h, \phi_\ell) & \Lambda(\phi_h, \tau_\ell) & \Lambda(\phi_h, \theta_\ell) \\ \Lambda(\tau_h, r_\ell) & \Lambda(\tau_h, \phi_\ell) & \Lambda(\tau_h, \tau_\ell) & \Lambda(\tau_h, \theta_\ell) \\ \Lambda(\theta_h, r_\ell) & \Lambda(\theta_h, \phi_\ell) & \Lambda(\theta_h, \tau_\ell) & \Lambda(\theta_h, \theta_\ell) \end{bmatrix} \tag{7}$$

with $h, \ell = 0, \ldots, K$. Substituting $\boldsymbol{Y}$ from (4) in (7) and accounting for the noise statistics yields

$$\Lambda(\boldsymbol{\gamma}_h, \boldsymbol{\gamma}_\ell) = \frac{2}{\sigma^2} \sum_{g=1}^{G} \sum_{n=0}^{N-1} \Re \left\{ \left(\frac{\partial m^g[n]}{\partial \boldsymbol{\gamma}_h} \right)^{\mathrm{H}} \frac{\partial m^g[n]}{\partial \boldsymbol{\gamma}_\ell} \right\} \quad (8)$$

with $\Re\{\cdot\}$ denoting the real-part operator and the noise-free observation at subcarrier n, transmission g is $m^g[n] = \sqrt{N_{\mathrm{BS}}} \sum_{k=0}^{K} \alpha_k \exp \left(\frac{-j 2\pi n \tau_k}{N T_S} \right) \boldsymbol{a}_{\mathrm{BS}}^{\mathrm{H}}(\theta_k) \boldsymbol{z}^g[n]$. We report in Appendix A the value of each entry of $\boldsymbol{\Lambda}(\boldsymbol{\gamma}_h, \boldsymbol{\gamma}_\ell)$. Two paths h and ℓ are said to be orthogonal when $\boldsymbol{\Lambda}(\boldsymbol{\gamma}_h, \boldsymbol{\gamma}_\ell) = \boldsymbol{0}_{4 \times 4}$ [39], with $\boldsymbol{0}_{L \times L}$ a $L \times L$ matrix of zeros.

B. FIM on Position Parameters

In this section, we derive the FIM in the position domain by applying a transformation of variables from the vector of channel parameters $\boldsymbol{\gamma}$ to a new vector of location parameters $\boldsymbol{\eta} = [\boldsymbol{\eta}_0^{\mathrm{T}} \cdots \boldsymbol{\eta}_K^{\mathrm{T}}]^{\mathrm{T}}$, where $\boldsymbol{\eta}_0 = [r_0 \ \phi_0 \ p_x \ p_y]^{\mathrm{T}}$ and $\boldsymbol{\eta}_k = [r_k \ \phi_k \ s_{k,x} \ s_{k,y}]^{\mathrm{T}}$, for $k \geq 1$. Specifically, by exploiting the geometric relationships between the parameters in $\boldsymbol{\gamma}$ and $\boldsymbol{\eta}$, we have

$$\tau_0 = \|\boldsymbol{p}\|/c \quad (9)$$
$$\theta_0 = \mathrm{atan2}(p_y, p_x) \quad (10)$$
$$\tau_k = \|\boldsymbol{s}_k\|/c + \|\boldsymbol{p} - \boldsymbol{s}_k\|/c, \ k \geq 1 \quad (11)$$
$$\theta_k = \mathrm{atan2}(s_{k,y}, s_{k,x}), \ k \geq 1, \quad (12)$$

where the function $\mathrm{atan2}(y, x)$ is the four-quadrant inverse tangent, and the angles are measured counterclockwise with respect to the x-axis.

The FIM in the position space $\boldsymbol{\eta}$ is obtained by means of the $4(K+1) \times 4(K+1)$ transformation matrix $\boldsymbol{T}$ as

$$\boldsymbol{J}_{\boldsymbol{\eta}} = \boldsymbol{T} \boldsymbol{J}_{\boldsymbol{\gamma}} \boldsymbol{T}^{\mathrm{T}} \quad (13)$$

where

$$\boldsymbol{T} \stackrel{\text{def}}{=} \frac{\partial \boldsymbol{\gamma}^{\mathrm{T}}}{\partial \boldsymbol{\eta}} = \begin{bmatrix} \boldsymbol{T}_{0,0} & \ldots & \boldsymbol{T}_{K,0} \\ \vdots & \ddots & \vdots \\ \boldsymbol{T}_{0,K} & \ldots & \boldsymbol{T}_{K,K} \end{bmatrix}. \quad (14)$$

Each submatrix $\boldsymbol{T}_{h,\ell}, h, \ell = 0, \ldots, K$, is given by

$$\boldsymbol{T}_{h,\ell} \stackrel{\text{def}}{=} \frac{\partial \boldsymbol{\gamma}_h^{\mathrm{T}}}{\partial \boldsymbol{\eta}_\ell} = \begin{bmatrix} \partial r_h/\partial r_\ell & \partial \phi_h/\partial r_\ell & \partial \tau_h/\partial r_\ell & \partial \theta_h/\partial r_\ell \\ \partial r_h/\partial \phi_\ell & \partial \phi_h/\partial \phi_\ell & \partial \tau_h/\partial \phi_\ell & \partial \theta_h/\partial \phi_\ell \\ \partial r_h/\partial \boldsymbol{s}_\ell & \partial \phi_h/\partial \boldsymbol{s}_\ell & \partial \tau_h/\partial \boldsymbol{s}_\ell & \partial \theta_h/\partial \boldsymbol{s}_\ell \end{bmatrix}$$
$$= \begin{bmatrix} \delta_{h\ell} & 0 & 0 & 0 \\ 0 & \delta_{h\ell} & 0 & 0 \\ 0 & 0 & \partial \tau_h/\partial \boldsymbol{s}_\ell & \partial \theta_h/\partial \boldsymbol{s}_\ell \end{bmatrix} \quad (15)$$

where $\delta_{h\ell}$ is the Kronecker symbol and

$$\frac{\partial \tau_0}{\partial \boldsymbol{p}} = \frac{1}{c} \left[\frac{p_x}{\|\boldsymbol{p}\|} \ \frac{p_y}{\|\boldsymbol{p}\|} \right]^{\mathrm{T}}$$

$$\frac{\partial \theta_0}{\partial \boldsymbol{p}} = \left[\frac{-p_y/p_x^2}{1 + (p_y/p_x)^2} \ \frac{1/p_x}{1 + (p_y/p_x)^2} \right]^{\mathrm{T}}$$

$$\frac{\partial \tau_h}{\partial \boldsymbol{p}} = \frac{1}{c} \left[\frac{p_x - s_{h,x}}{\|\boldsymbol{p} - \boldsymbol{s}_h\|} \ \frac{p_y - s_{h,y}}{\|\boldsymbol{p} - \boldsymbol{s}_h\|} \right]^{\mathrm{T}}$$

$$\frac{\partial \tau_h}{\partial \boldsymbol{s}_h} = \frac{1}{c} \left[\left(\frac{s_{h,x}}{\|\boldsymbol{s}_h\|} - \frac{(p_x - s_{h,x})}{\|\boldsymbol{p} - \boldsymbol{s}_h\|} \right) \left(\frac{s_{h,y}}{\|\boldsymbol{s}_k\|} - \frac{(p_y - s_{h,y})}{\|\boldsymbol{p} - \boldsymbol{s}_h\|} \right) \right]^{\mathrm{T}}$$

$$\frac{\partial \theta_h}{\partial \boldsymbol{s}_h} = \left[\frac{-s_{h,y}/s_{h,x}^2}{1 + (s_{h,y}/s_{h,x})^2} \ \frac{1/s_{h,x}}{1 + (s_{h,y}/s_{h,x})^2} \right]^{\mathrm{T}},$$

with the last two equations meant for $h \neq 0$, and $\boldsymbol{T}_{h,\ell} = \boldsymbol{0}_{4 \times 4}$ for $\ell \geq 1$ and $\ell \neq h$. The FIM $\boldsymbol{J}_{\boldsymbol{\eta}}$ is invertible when both $\boldsymbol{J}_{\boldsymbol{\gamma}}$ and $\boldsymbol{T}$ are invertible (sufficient but not necessary condition), due to the one-to-one mapping between channel and location parameters.

C. Bounds on MS Position Estimation Error

To derive the lower bound on the uncertainty of MS position estimation, we consider the CRLB in the location domain obtained by inverting the FIM $\boldsymbol{J}_{\boldsymbol{\eta}}$ in (13), i.e., $\boldsymbol{\Sigma}_{\boldsymbol{\eta}} = \boldsymbol{J}_{\boldsymbol{\eta}}^{-1}$. Specifically, the position error bound (PEB) is computed by adding the third and fourth diagonal entries of the $\boldsymbol{\Sigma}_{\boldsymbol{\eta}}$ matrix, and taking the square root as

$$\mathrm{PEB} = \sqrt{[\boldsymbol{\Sigma}_{\boldsymbol{\eta}}]_{3,3} + [\boldsymbol{\Sigma}_{\boldsymbol{\eta}}]_{4,4}} \quad (16)$$

where $[\cdot]_{j,j}$ selects the j-th diagonal entry of $\boldsymbol{\Sigma}_{\boldsymbol{\eta}}$.

D. Role of NLOS Components on MS Position Estimation

In the previous subsections, we have derived the fundamental bounds on the estimation of the unknown channel and position parameters. Based on that, we now discuss how the presence of NLOS paths impacts on the estimation of the MS position $\boldsymbol{p}$ under the considered MISO setup. We start by recalling that the CRLB matrix $\boldsymbol{\Sigma}_{\boldsymbol{\eta}}$ matrix is given by $\boldsymbol{\Sigma}_{\boldsymbol{\eta}} = (\boldsymbol{T} \boldsymbol{J}_{\boldsymbol{\gamma}} \boldsymbol{T}^{\mathrm{T}})^{-1}$. Focusing on the vectors $\boldsymbol{\gamma}_k$ and $\boldsymbol{\eta}_k$ of the k-th path, it is interesting to note that the number of parameters in both channel and location domains is the same, and there exists a bijective relationship between them (see eqs. (9)–(12)). Consequently, $\boldsymbol{\Sigma}_{\boldsymbol{\eta}}$ can be equivalently expressed as $\boldsymbol{\Sigma}_{\boldsymbol{\eta}} = (\boldsymbol{T}^{-1})^{\mathrm{T}} \boldsymbol{J}_{\boldsymbol{\gamma}}^{-1} \boldsymbol{T}^{-1}$, where, by invoking the multivariate inverse function theorem, the inverse transformation matrix $\boldsymbol{T}^{-1}$ can be directly computed as the derivative of the location parameters with respect to the channel parameters, i.e.,

$$\boldsymbol{T}^{-1} = \frac{\partial \boldsymbol{\eta}^{\mathrm{T}}}{\partial \boldsymbol{\gamma}} = \begin{bmatrix} \bar{\boldsymbol{T}}_{0,0} & \ldots & \bar{\boldsymbol{T}}_{K,0} \\ \vdots & \ddots & \vdots \\ \bar{\boldsymbol{T}}_{0,K} & \ldots & \bar{\boldsymbol{T}}_{K,K} \end{bmatrix} \quad (17)$$

with each 4×4 block $\bar{\boldsymbol{T}}_{h,\ell}, h, \ell = 0, \ldots, K$, obtained as

$$\bar{\boldsymbol{T}}_{h,\ell} \stackrel{\text{def}}{=} \frac{\partial \boldsymbol{\eta}_h^{\mathrm{T}}}{\partial \boldsymbol{\gamma}_\ell} = \begin{bmatrix} \delta_{h\ell} & 0 & 0 \\ 0 & \delta_{h\ell} & 0 \\ 0 & 0 & \partial \boldsymbol{s}_h/\partial \tau_\ell \\ 0 & 0 & \partial \boldsymbol{s}_h/\partial \theta_\ell \end{bmatrix}. \quad (18)$$

By noting that the blocks $\bar{\boldsymbol{T}}_{h,\ell} = \boldsymbol{0}_{4\times 4}$ for $l \geq 1$ and $h \neq \ell$, it follows that

$$\boldsymbol{\Sigma}_{\boldsymbol{\eta}} = \begin{bmatrix} \bar{\boldsymbol{T}}_{0,0}^{\mathrm{T}} & \boldsymbol{0}_{4\times 4} & \cdots & \boldsymbol{0}_{4\times 4} \\ \bar{\boldsymbol{T}}_{1,0}^{\mathrm{T}} & \bar{\boldsymbol{T}}_{1,1}^{\mathrm{T}} & \cdots & \boldsymbol{0}_{4\times 4} \\ \vdots & \vdots & \ddots & \vdots \\ \bar{\boldsymbol{T}}_{K,0}^{\mathrm{T}} & \boldsymbol{0}_{4\times 4} & \cdots & \bar{\boldsymbol{T}}_{K,K}^{\mathrm{T}} \end{bmatrix} \boldsymbol{J}_{\boldsymbol{\gamma}}^{-1} \begin{bmatrix} \bar{\boldsymbol{T}}_{0,0} & \bar{\boldsymbol{T}}_{1,0} & \cdots & \bar{\boldsymbol{T}}_{K,0} \\ \boldsymbol{0}_{4\times 4} & \bar{\boldsymbol{T}}_{1,1} & \cdots & \boldsymbol{0}_{4\times 4} \\ \vdots & \vdots & \ddots & \vdots \\ \boldsymbol{0}_{4\times 4} & \boldsymbol{0}_{4\times 4} & \cdots & \bar{\boldsymbol{T}}_{K,K} \end{bmatrix} \tag{19}$$

This leads us to our first main result.

Theorem 1. *Denoting by PEB_k the value of the PEB when k NLOS paths with unknown origin besides the LOS path are present, with $0 \leq k \leq K$, then*

$$\mathrm{PEB}_K \geq \mathrm{PEB}_0, \tag{20}$$

with equality when all paths are orthogonal.

Proof. We first prove the inequality. We denote the $K+1$ 4×4 diagonal blocks of $\boldsymbol{J}_{\boldsymbol{\gamma}}^{-1}$ by $\boldsymbol{C}_0, \ldots, \boldsymbol{C}_K$. From the Schur complement, it follows that $\boldsymbol{C}_k \succeq (\boldsymbol{\Lambda}(\boldsymbol{\gamma}_k, \boldsymbol{\gamma}_k))^{-1}$. From (16), it is evident that the relevant information on the estimation of $\boldsymbol{p}$ resides in the first 4×4 block of $\boldsymbol{\Sigma}_{\boldsymbol{\eta}}$. By taking the products in (19), it turns out that such a block is equal to $\bar{\boldsymbol{T}}_{0,0}^{\mathrm{T}} \boldsymbol{C}_0 \bar{\boldsymbol{T}}_{0,0} \succeq \bar{\boldsymbol{T}}_{0,0}^{\mathrm{T}} (\boldsymbol{\Lambda}(\boldsymbol{\gamma}_0, \boldsymbol{\gamma}_0))^{-1} \bar{\boldsymbol{T}}_{0,0}$. Applying the PEB definition in (16) to both sides of this inequality, it turns out that $\mathrm{PEB}_K \geq \mathrm{PEB}_0$.

We now prove the equality when paths are orthogonal. Under typical mmWave conditions, the different received paths can be resolved either in the angular or time domains, with practically negligible overlap among them. In other words, the NLOS paths can be treated as orthogonal paths carrying independent information [9], [40], leading in turn to $\boldsymbol{\Lambda}(\boldsymbol{\gamma}_h, \boldsymbol{\gamma}_\ell) = \boldsymbol{0}_{4\times 4}$ for $h \neq \ell$ in (6). Neglecting these terms, the approximate expression of $\boldsymbol{\Sigma}_{\boldsymbol{\eta}}$ is given by (21), where now $\boldsymbol{C}_k = (\boldsymbol{\Lambda}(\boldsymbol{\gamma}_k, \boldsymbol{\gamma}_k))^{-1}$. It then immediately follows that $\mathrm{PEB}_K = \mathrm{PEB}_0$. □

This effect relates to the fact that the MS is equipped with a single-antenna receiver, hence it cannot exploit the NLOS parameters to gain additional position-related information (i.e., AOAs). This represents a major difference compared to the MIMO setup where, in general, the contribution of the NLOS components can result in a reduction of the PEB [2], [10]. In the MISO case, multipath propagation will degrade the MS localization only when the NLOS paths and the LOS significantly overlap, but will never improve the PEB compared to the LOS-only case. From such considerations, it also follows that in the MISO setup (i) localization without LOS is not possible; and (ii) the NLOS paths cannot be used to synchronize the MS to the BS. Both aspects are in contrast to the MIMO case, as shown in [41].

Remarkably, we observe from (21) that mapping of the scatterers positions is still possible in spite of the fact that the receiver has only a single antenna, that is, it cannot perform any spatial processing. More specifically, the terms in the main diagonal of (21) reveal that the accuracy in the estimation of each scatterer's position $\boldsymbol{s}_k$ is linked to the parameters of the associated k-th NLOS path $\bar{\boldsymbol{T}}_{k,k}^{\mathrm{T}} \boldsymbol{C}_k \bar{\boldsymbol{T}}_{k,k}$, as well as to the parameters related to the LOS link $\bar{\boldsymbol{T}}_{k,0}^{\mathrm{T}} \boldsymbol{C}_0 \bar{\boldsymbol{T}}_{k,0}$. Given the additive nature of such terms, the lower the uncertainty in

the LOS parameters, the higher the accuracy in mapping the multipath environment.

A direct consequence of the above analysis is that, given the considered model, the MS position can be refined using the information from the NLOS paths only in case the scatterers' positions are known a priori. In fact, in the latter case the FIM analysis can be further specialized considering a reduced vector of unknown location parameters $\boldsymbol{\eta} = \boldsymbol{\eta}_0$. Accordingly, the FIM in the position space $\boldsymbol{\eta}_0$ is obtained by means of a reduced $4 \times 4(K+1)$ transformation matrix $\boldsymbol{T}$ as

$$\boldsymbol{J}_{\boldsymbol{\eta}_0} = \begin{bmatrix} \boldsymbol{T}_{0,0} & \cdots & \boldsymbol{T}_{K,0} \end{bmatrix} \boldsymbol{J}_{\boldsymbol{\gamma}} \begin{bmatrix} \boldsymbol{T}_{0,0}^{\mathrm{T}} \\ \boldsymbol{T}_{1,0}^{\mathrm{T}} \\ \vdots \\ \boldsymbol{T}_{K,0}^{\mathrm{T}} \end{bmatrix}.$$

After simple matrix multiplications, it follows that

$$\boldsymbol{J}_{\boldsymbol{\eta}_0} = \sum_{k=0}^{K} \left(\boldsymbol{T}_{k,0} \boldsymbol{\Lambda}(\boldsymbol{\gamma}_k, \boldsymbol{\gamma}_0) \boldsymbol{T}_{0,0}^{\mathrm{T}} + \ldots + \boldsymbol{T}_{k,0} \boldsymbol{\Lambda}(\boldsymbol{\gamma}_k, \boldsymbol{\gamma}_K) \boldsymbol{T}_{K,0}^{\mathrm{T}} \right).$$

By exploiting also in this case the hypothesis of orthogonality among paths, in the above summation only the blocks $\boldsymbol{\Lambda}(\boldsymbol{\gamma}_k, \boldsymbol{\gamma}_k) \neq \boldsymbol{0}$, so that the FIM can be approximated as

$$\boldsymbol{J}_{\boldsymbol{\eta}_0} = \sum_{k=0}^{K} \boldsymbol{T}_{k,0} \boldsymbol{C}_k^{-1} \boldsymbol{T}_{k,0}^{\mathrm{T}}.$$

The above expression reveals that, in presence of scatterers with known positions, the NLOS paths increase the amount of information available for the estimation of the MS position.

IV. JOINT MAXIMUM LIKELIHOOD LOCALIZATION AND MAPPING

In this section, we present the joint maximum likelihood (ML) estimator, a low-complexity channel estimator working in two dimensions, and the localization and mapping algorithm. We also show that the ML estimator can be performed equivalently in the position domain, and provide insights into the obtained solutions.

A. Maximum Likelihood Estimation of Channel Parameters

We start the derivation by noting that each received signal $y^g[n]$, $1 \leq g \leq G$, $0 \leq n \leq N-1$, can be statistically characterized as

$$y^g[n] \sim \mathcal{CN}(\sqrt{N_{\mathrm{BS}}} \bar{\boldsymbol{h}}^{\mathrm{T}}[n] \boldsymbol{z}^g[n], \sigma^2) \tag{22}$$

where $\bar{\boldsymbol{h}}^{\mathrm{T}}[n] = \sum_{k=0}^{K} \alpha_k e^{\frac{-j 2 \pi n \tau_k}{N T_S}} \boldsymbol{a}_{\mathrm{BS}}^{\mathrm{H}}(\theta_k)$ and all the parameters are treated as deterministic unknowns, except the transmitted symbols $\boldsymbol{z}^g[n]$, which are assumed known to the receiver, and the number of paths K, which can be determined during the initial access phase [42], [43]. To formulate the estimation problem, we re-order the unknown parameters as $\boldsymbol{\varphi} = [\boldsymbol{\Theta}^{\mathrm{T}} \boldsymbol{\psi}^{\mathrm{T}}]^{\mathrm{T}}$, where $\boldsymbol{\Theta} = [\theta_0 \ \tau_0 \ \cdots \ \theta_K \ \tau_K]^{\mathrm{T}}$ represents the parameters of interest linked to the desired MS and scatterers positions, while $\boldsymbol{\psi} = [\sigma^2 \ \boldsymbol{\alpha}^{\mathrm{T}}]^{\mathrm{T}}$ with $\boldsymbol{\alpha} = [\alpha_0 \ \cdots \ \alpha_K]^{\mathrm{T}}$ denotes the vector of nuisance parameters. Notice that, differently from the LOS-only scenario, including the NLOS

$$\boldsymbol{\Sigma_\eta} \approx \begin{bmatrix} \bar{\boldsymbol{T}}_{0,0}^{\mathrm{T}}\boldsymbol{C}_0\bar{\boldsymbol{T}}_{0,0} & \bar{\boldsymbol{T}}_{0,0}^{\mathrm{T}}\boldsymbol{C}_0\bar{\boldsymbol{T}}_{1,0} & \bar{\boldsymbol{T}}_{0,0}^{\mathrm{T}}\boldsymbol{C}_0\bar{\boldsymbol{T}}_{2,0} & \cdots & \bar{\boldsymbol{T}}_{0,0}^{\mathrm{T}}\boldsymbol{C}_0\bar{\boldsymbol{T}}_{K,0} \\ \bar{\boldsymbol{T}}_{1,0}^{\mathrm{T}}\boldsymbol{C}_0\bar{\boldsymbol{T}}_{0,0} & \bar{\boldsymbol{T}}_{1,0}^{\mathrm{T}}\boldsymbol{C}_0\bar{\boldsymbol{T}}_{1,0} + \bar{\boldsymbol{T}}_{1,1}^{\mathrm{T}}\boldsymbol{C}_1\bar{\boldsymbol{T}}_{1,1} & \bar{\boldsymbol{T}}_{1,0}^{\mathrm{T}}\boldsymbol{C}_0\bar{\boldsymbol{T}}_{2,0} & \cdots & \bar{\boldsymbol{T}}_{1,0}^{\mathrm{T}}\boldsymbol{C}_0\bar{\boldsymbol{T}}_{K,0} \\ \bar{\boldsymbol{T}}_{2,0}^{\mathrm{T}}\boldsymbol{C}_0\bar{\boldsymbol{T}}_{0,0} & \bar{\boldsymbol{T}}_{2,0}^{\mathrm{T}}\boldsymbol{C}_0\bar{\boldsymbol{T}}_{1,0} & \bar{\boldsymbol{T}}_{2,0}^{\mathrm{T}}\boldsymbol{C}_0\bar{\boldsymbol{T}}_{2,0} + \bar{\boldsymbol{T}}_{2,2}^{\mathrm{T}}\boldsymbol{C}_2\bar{\boldsymbol{T}}_{2,2} & \cdots & \bar{\boldsymbol{T}}_{2,0}^{\mathrm{T}}\boldsymbol{C}_0\bar{\boldsymbol{T}}_{K,0} \\ \vdots & \vdots & \vdots & \ddots & \vdots \\ \bar{\boldsymbol{T}}_{K,0}^{\mathrm{T}}\boldsymbol{C}_0\bar{\boldsymbol{T}}_{0,0} & \bar{\boldsymbol{T}}_{K,0}^{\mathrm{T}}\boldsymbol{C}_0\bar{\boldsymbol{T}}_{1,0} & \bar{\boldsymbol{T}}_{K,0}^{\mathrm{T}}\boldsymbol{C}_0\bar{\boldsymbol{T}}_{2,0} & \cdots & \bar{\boldsymbol{T}}_{K,0}^{\mathrm{T}}\boldsymbol{C}_0\bar{\boldsymbol{T}}_{K,0} + \bar{\boldsymbol{T}}_{K,K}^{\mathrm{T}}\boldsymbol{C}_K\bar{\boldsymbol{T}}_{K,K} \end{bmatrix} \quad (21)$$

links in the localization process introduces additional unknown parameters that make the resulting estimation problem much more challenging. Following the ML criterion, the estimation problem can be thus formulated as

$$\hat{\boldsymbol{\Theta}} = \arg\max_{\boldsymbol{\Theta}}[\max_{\boldsymbol{\psi}} L(\boldsymbol{\Theta}, \boldsymbol{\psi})] \quad (23)$$

where $L(\boldsymbol{\Theta}, \boldsymbol{\psi}) \overset{\text{def}}{=} \log f(\boldsymbol{Y}|\boldsymbol{\Theta}, \boldsymbol{\psi})$ and $f(\cdot)$ denotes the probability density function of the observations $\boldsymbol{Y}$ given $\boldsymbol{\psi}$ and $\boldsymbol{\Theta}$. A more convenient rewriting of the channel model in (1) allows us to express the likelihood in (23) as

$$L(\boldsymbol{\Theta}, \boldsymbol{\psi}) = -NG\log(\pi\sigma^2)$$
$$- \frac{1}{\sigma^2}\sum_{g=1}^{G} \|\boldsymbol{y}^g - \sqrt{N_{\mathrm{BS}}}\boldsymbol{Q}^g\boldsymbol{\alpha}\|^2 \quad (24)$$

where

$$\boldsymbol{Q}^g = \begin{bmatrix} (\boldsymbol{z}^g[0])^{\mathrm{T}}\boldsymbol{D}[0] \\ \vdots \\ (\boldsymbol{z}^g[N-1])^{\mathrm{T}}\boldsymbol{D}[N-1] \end{bmatrix} \in \mathbb{C}^{N\times(K+1)} \quad (25)$$

with $\boldsymbol{y}^g = [y^g[0]\, y^g[1]\, \cdots\, y^g[N-1]]^{\mathrm{T}}$ the g-th column of the observation matrix $\boldsymbol{Y}$, and

$$\boldsymbol{D}[n] = \begin{bmatrix} \mathrm{e}^{\frac{-j2\pi n\tau_0}{NT_S}}\boldsymbol{a}_{\mathrm{BS}}^*(\theta_0) & \cdots & \mathrm{e}^{\frac{-j2\pi n\tau_K}{NT_S}}\boldsymbol{a}_{\mathrm{BS}}^*(\theta_K) \end{bmatrix}. \quad (26)$$

It is easy to observe that the noise variance can be estimated as $\hat{\sigma}^2 = \sum_{g=1}^{G}\|\boldsymbol{y}^g - \sqrt{N_{\mathrm{BS}}}\boldsymbol{Q}^g\boldsymbol{\alpha}\|^2/(NG)$, leading to the compressed likelihood

$$L_K(\boldsymbol{\Theta}, \boldsymbol{\alpha}) = \sum_{g=1}^{G} \|\boldsymbol{y}^g - \sqrt{N_{\mathrm{BS}}}\boldsymbol{Q}^g\boldsymbol{\alpha}\|^2 \quad (27)$$

where $L_K(\boldsymbol{\Theta}, \boldsymbol{\alpha})$ is the compressed negative log-likelihood function in presence of K NLOS paths. Eq. (27) can be optimized with respect to the entire vector $\boldsymbol{\alpha} \in \mathbb{C}^{(K+1)\times 1}$, yielding $\hat{\boldsymbol{\alpha}} = 1/\sqrt{N_{\mathrm{BS}}}\boldsymbol{Q}^{-1}\sum_{g=1}^{G}(\boldsymbol{Q}^g)^{\mathrm{H}}\boldsymbol{y}^g$ where $\boldsymbol{Q} = \sum_{g=1}^{G}(\boldsymbol{Q}^g)^{\mathrm{H}}\boldsymbol{Q}^g$. Substituting these minimizing values back in (27) leads to

$$L_K(\boldsymbol{\Theta}) = \sum_{g=1}^{G} \|\boldsymbol{y}^g - \boldsymbol{Q}^g(\boldsymbol{\Theta})\hat{\boldsymbol{\alpha}}(\boldsymbol{\Theta})\|^2 \quad (28)$$

and, accordingly, the final joint ML estimator is given by

$$\hat{\boldsymbol{\Theta}} = \arg\min_{\boldsymbol{\Theta}} L_K(\boldsymbol{\Theta}). \quad (29)$$

The cost function (28) is highly non-linear in the $2(K+1)$ unknown parameters and does not admit a closed-form solution or a multidimensional exhaustive search. Therefore, the joint ML need to be solved by resorting to iterative numerical optimization routines such as, for instance, those based on

derivatives of the cost function (e.g., gradient descent or its variants [44]), or by employing more direct approaches such as the Nelder-Mead method [45], starting from a good initial estimate.

B. Low-complexity Channel Parameter Estimation

To solve the channel parameter estimation problem in practice, we take advantage of the sparse nature of the mmWave channel and propose a reduced-complexity suboptimal approach to obtain a good initial estimate of $\boldsymbol{\Theta}$. The main idea consists in exploiting the fact that the received paths are almost orthogonal between each other, as discussed in Sec. III-D. Under this assumption, the joint ML estimation problem can be approximated to a problem of multiple single-path estimation, where each path can be described by the following simplified channel model

$$\tilde{\boldsymbol{h}}^{\mathrm{T}}[n] = \alpha e^{\frac{-j2\pi n\tau}{NT_S}}\boldsymbol{a}_{\mathrm{BS}}^{\mathrm{H}}(\theta), \quad n = 0,\ldots,N-1 \quad (30)$$

with α, θ and τ complex amplitude, AOD and TOF of a single path, respectively. Replacing (1) with (30) in the derivation of the joint ML immediately leads to the cost function of the single-path ML estimator, denoted as $L_0(\theta, \tau)$, whose expression can be straightforwardly obtained as a special case of (28) for $\boldsymbol{\Theta} = [\theta\ \tau]^{\mathrm{T}}$, which is tantamount to considering $K = 0$ in the original joint ML estimation problem.

In analogy to traditional subspace-based AOA estimation, we leverage orthogonality among the paths and interpret $L_0(\theta, \tau)$ as a kind of "pseudospectrum", whose minima occur in correspondence of pairs (θ, τ) close to the actual channel parameters θ_k and τ_k of each k-th path. As it will be shown in Sec. V, searching for the $K+1$ dominant minima in $L_0(\theta, \tau)$ and using these as initial estimates in the iterative minimization of $L_K(\boldsymbol{\Theta})$ can efficiently solve the joint ML estimation problem and attain the theoretical performance bounds, but at the significantly reduced cost of a coarse two-dimensional search over the space (θ, τ) instead of a prohibitive $2(K+1)$-dimensional search.

C. Localization and Mapping

From the theoretical analysis conducted in Sec. III-D, it emerged that in a MISO setup, NLOS components cannot be harnessed to determine the unknown MS position. In this respect, the natural way to obtain an estimate of $\boldsymbol{p}$ is to exploit the sole LOS position-related parameters, which can be identified among the $K+1$ estimated pairs $(\hat{\theta}_k, \hat{\tau}_k)$ as the pair with the minimum value for $\hat{\tau}_k$, while the remaining pairs are used for determining the map.

1) Localization: In the following, we will refer to such estimates as $(\hat{\theta}_{\mathrm{LOS}}, \hat{\tau}_{\mathrm{LOS}})$. The unknown MS position can be then determined by solving (9)–(10) for $\boldsymbol{p}$:

$$\hat{\boldsymbol{p}} = c\hat{\tau}_{\mathrm{LOS}}[\cos\hat{\theta}_{\mathrm{LOS}} \ \sin\hat{\theta}_{\mathrm{LOS}}]^{\mathrm{T}}. \qquad (31)$$

2) Mapping: Once the estimate $\hat{\boldsymbol{p}}$ is obtained, it can be used in conjunction with each pair $(\hat{\theta}_k, \hat{\tau}_k)$, $k \geq 1$, to retrieve the related scatterer's position $\boldsymbol{s}_k$. More precisely, the direction $\hat{\theta}_k$ constrains the sought $\hat{\boldsymbol{s}}_k$ to lie on the straight line passing by the BS position and having angular coefficient $m(\hat{\theta}_k) = \tan(\hat{\theta}_k)$. Among all the possible candidate positions on that line, $\hat{\boldsymbol{s}}_k$ is the one also satisfying the distance constraint $\hat{d}_k = c\hat{\tau}_k$ with $\hat{\boldsymbol{p}}$. In formulas, we have that

$$\sqrt{\hat{s}_{k,x}^2(1 + m(\hat{\theta}_k)^2) - 2(\hat{p}_x + m(\hat{\theta}_k)\hat{p}_y)\hat{s}_{k,x} + \|\hat{\boldsymbol{p}}\|^2}$$
$$+ \sqrt{\hat{s}_{k,x}^2(1 + m(\hat{\theta}_k)^2)} = c\hat{\tau}_k \qquad (32)$$

with $\hat{s}_{k,y} = m(\hat{\theta}_k)\hat{s}_{k,x}$. Assuming for simplicity that $\hat{s}_{k,x} > 0 \ \forall k = 1, \ldots, K$, the position of the k-th scatterer can be estimated in closed-form as

$$\begin{cases} \hat{s}_{k,x} = \frac{1}{2}\frac{(c\hat{\tau}_k)^2 - \hat{p}_x^2 - \hat{p}_y^2}{\sqrt{1+\tan^2(\hat{\theta}_k)}\,c\hat{\tau}_k - \hat{p}_x - \tan(\hat{\theta}_k)\hat{p}_y} \\ \hat{s}_{k,y} = \tan(\hat{\theta}_k)\hat{s}_{k,x} \end{cases}.$$

We observe that, in line with the theoretical findings in Sec. III-D, the accuracy on the estimation of $\boldsymbol{s}_k$ depends on the quality of the NLOS parameters estimates $\hat{\theta}_k$ and $\hat{\tau}_k$, as well as on the goodness of $\hat{\boldsymbol{p}}$, which is estimated based on the LOS-only parameters $\hat{\tau}_{\mathrm{LOS}}$ and $\hat{\theta}_{\mathrm{LOS}}$. Given the nonlinear nature of the geometric estimator (IV-C2), it is not trivial to figure out how the involved parameters impact the estimation of $\hat{\boldsymbol{s}}_k$. The proposed solution is summarized in Algorithm 1.

Algorithm 1: Proposed reduced-complexity algorithm

Input: $\boldsymbol{Y}, K$
Output: $\hat{\boldsymbol{p}}, \hat{\boldsymbol{s}}_1, \ldots, \hat{\boldsymbol{s}}_K$

1 **for** *i from 0 to K* **do**
2   Compute the single-path "pseudospectrum" function $L_0(\theta, \tau)$
3     $[\hat{\theta}_i \ \hat{\tau}_i] = \arg\min\limits_{(\theta_i, \tau_i)} L_0(\theta, \tau)$
4 **end**
5 $\hat{\boldsymbol{\Theta}}_{\mathrm{init}} = \begin{bmatrix} \hat{\theta}_0 & \hat{\tau}_0 & \cdots & \hat{\theta}_K & \hat{\tau}_K \end{bmatrix}^{\mathrm{T}}$
6 $\hat{\boldsymbol{\Theta}} = \mathrm{IterativeMin}(L_K(\boldsymbol{\Theta}), \hat{\boldsymbol{\Theta}}_{\mathrm{init}})$
7 Select $(\hat{\theta}_{\mathrm{LOS}}, \hat{\tau}_{\mathrm{LOS}})$ as the pair $(\hat{\theta}_k, \hat{\tau}_k)$ with minimum $\hat{\tau}_k$
8 $\hat{\boldsymbol{p}} = c\hat{\tau}_{\mathrm{LOS}}[\cos\hat{\theta}_{\mathrm{LOS}} \ \sin\hat{\theta}_{\mathrm{LOS}}]^{\mathrm{T}}$
9 **for** *i from 1 to K* **do**
10     $\hat{s}_{k,x} = \frac{1}{2}\frac{(c\hat{\tau}_k)^2 - \hat{p}_x^2 - \hat{p}_y^2}{\sqrt{1+\tan^2(\hat{\theta}_k)}\,c\hat{\tau}_k - \hat{p}_x - \tan(\hat{\theta}_k)\hat{p}_y}$
11     $\hat{s}_{k,y} = \tan(\hat{\theta}_k)\hat{s}_{k,x}$
12 **end**

Two comments are now in order. First, it is worth noting that, unlike the MIMO case, in the considered mmWave MISO setup the LOS path must be present in order for the single-snapshot localization and mapping problem to be solvable. To avoid a wrong estimation of the MS and scatterers positions in

case of pure NLOS propagation, a preliminary NLOS detection step should be performed before applying the proposed two-step procedure, e.g. using state-of-the-art approaches such as [46], [47]. Second, notice that the initialization of the algorithm can be replaced by a different channel estimation method, e.g. subspace-based methods. However, the advantage of the proposed algorithm is that it exploits the quasi-orthogonality of the signals in the joint space-time domain to reduce the complexity to a single-path estimation. As a consequence, simultaneous localization and mapping can feasibly be implemented even in a simple one-antenna mmWave receiver using only a single snapshot (by comparison, subspace-based methods require accumulating a significant number of snapshots to blindly estimate the whole subspaces, and have the additional complexity of eigendecomposition).

D. Equivalence of Maximum Likelihood Estimation in Channel and Position Domains

In this section, we briefly discuss an alternative formulation of the ML estimation problem in the position domain, showing that the resulting estimator is equivalent to the one in the channel domain. Without loss of generality, we focus on the single-path cost function $L_0(\theta, \tau)$, but the same reasoning can be easily applied also to $L_K(\boldsymbol{\Theta})$. More precisely, by expressing the channel parameters θ and τ as a function of their corresponding location parameters according to (9)–(10), (30) can be equivalently rewritten as

$$\tilde{\boldsymbol{h}}^{\mathrm{T}}[n] = \alpha e^{\frac{-j2\pi n\|\boldsymbol{s}\|}{cNT_S}} \boldsymbol{a}_{\mathrm{BS}}^{\mathrm{H}}(\mathrm{atan2}(s_y, s_x)), \quad n = 0, \ldots, N-1 \qquad (33)$$

where $\boldsymbol{s} = \boldsymbol{g}(\theta, \tau) = c\tau[\cos\theta \ \sin\theta]^{\mathrm{T}}$ and $\boldsymbol{g}(\cdot)$ is the bijective mapping (transformation from polar to Cartesian coordinates) between the channel and position parameters. Accordingly, we denote by $L_0(\boldsymbol{s})$ the position-domain counterpart of the cost function $L_0(\theta, \tau)$. The equivalence between the ML formulations in both channel and position domains easily follows by observing that, given the bijective mapping $\boldsymbol{s} = \boldsymbol{g}(\theta, \tau)$, the likelihood $L_0(\theta, \tau)$ can be rewritten as a function of $\boldsymbol{s}$, i.e.,

$$L_0(\theta, \tau) = L_0(\boldsymbol{g}^{-1}(\boldsymbol{s})). \qquad (34)$$

Analogously to $L_0(\theta, \tau)$, searching for the $K+1$ dominant minima of $L_0(\boldsymbol{s})$ provides an initial estimate of the MS and scatterers positions, which can be subsequently used to solve the joint ML problem in the position domain. In this respect, it is worth noting that since the single-path model (33) is unable to capture the geometric reflections of the propagating rays, the bijective transformation $\boldsymbol{g}(\cdot)$ will map the TOF τ_k of each NLOS path into a position that falls within a distance $d_k = c\tau_k$ from the BS, along a direction identified by the AOD θ_k, thus leading to a final position that does not coincide with the actual position of the k-th scatterer. Let us denote by $\boldsymbol{s}_k^e = [s_{k,x}^e \ s_{k,y}^e]^{\mathrm{T}}$, $k \geq 1$, such "equivalent" positions. Then, each $\boldsymbol{s}_k^e$ can be mapped back to its corresponding position $\boldsymbol{s}_k$ by applying some geometric considerations: first, we write the parametric expression for the segment passing by the BS and the equivalent position $\boldsymbol{s}_k^e$, that is, $\boldsymbol{s}_k(\lambda) = \lambda\boldsymbol{p}_{\mathrm{BS}} + (1-\lambda)\boldsymbol{s}_k^e$, $\lambda \in [0, 1]$. Then, we retain as position $\boldsymbol{s}_k$ the point on the line

corresponding to the value λ^* satisfying $\|\boldsymbol{s}_k^e - \boldsymbol{s}_k(\lambda^*)\| = \|\boldsymbol{s}_k(\lambda^*) - \boldsymbol{p}\|$, that is

$$\lambda^* = \frac{1}{2} \frac{\|\boldsymbol{s}_k^e - \boldsymbol{p}\|^2}{\|\boldsymbol{s}_k^e\|^2 - (p_x s_{k,x}^e + p_y s_{k,y}^e)} \tag{35}$$

(where without loss of generality we kept assuming that the BS is placed at the origin of the reference system). Given the equivalence between the two estimators, in the following we present the results only for one of them; in particular, we opt for the joint ML in the channel domain, being closer to the physics of the channel hence more easily interpretable in terms of paths (i.e., angles and delays).

V. SIMULATION ANALYSIS AND RESULTS

In this section, we present a simulation analysis aimed at evaluating the performance of the proposed joint ML estimator, considering different values of the relevant parameters, also in comparison with the theoretical bounds derived in Sec. III. To evaluate the performance, we consider the Root Mean Squared Error (RMSE) estimated on the basis of 1000 Monte Carlo independent trials.

A. Simulation Setup

The analyzed scenario consists of a single BS equipped with $N_{\mathrm{BS}} = 20$ antennas, placed at a known position $\boldsymbol{p}_{\mathrm{BS}} = [3\ 0]^{\mathrm{T}}$ m, while the MS is located at $\boldsymbol{p} = [10\ 4]^{\mathrm{T}}$ m. The localization process is carried out by exploiting only a single broadcast signal in DL ($G = 1$) with bandwidth $B = 40$ MHz over a central frequency $f_c = 60$ GHz, using $N = 20$ different subcarriers. The simulations are carried out without assuming any a priori knowledge of the MS and scatterers positions; accordingly, we set the beamforming matrix $\boldsymbol{F}^g[n]$ to have $M = N_{\mathrm{BS}}/2$ uniformly-spaced beams that cover the whole considered area, and keep it constant over each transmission g and subcarrier n.

We compute the channel path loss ρ_k for each k-th path according to the geometry statistics in [48], [49]. To assess the algorithm performance under different operating conditions, we introduce the LOS-to-multipath ratio (LMR) $\mathrm{LMR}_k = P_{\mathrm{LOS}}/P_{\mathrm{NLOS}}^k$. This indicator reflects the theoretical insights provided by the CRLB analysis in Sec. III: indeed, from the diagonal elements of (21), we observed that the lower bounds on the estimation of each scatterer position $\boldsymbol{s}_k$ depend only on the parameters of the associated k-th NLOS path and on the parameters of the LOS path, hence the ratio between their powers represents a meaningful parameter to discriminate between favorable (i.e., stronger LOS) and unfavorable (i.e., weaker LOS) conditions. Accordingly, the total LMR is given by $\mathrm{LMR} = P_{\mathrm{LOS}}/\sum_{k=1}^{K} P_{\mathrm{NLOS}}^k$. The transmit power P_t adopted by the BS is varied (from about 0.1 mW up to about 10 mW) in order to obtain different ranges of SNR, defined as $\mathrm{SNR} \stackrel{\mathrm{def}}{=} 10 \log_{10}\left(P_t/(\rho_0 N_0 B)\right)$, where N_0 is the noise power spectral density and ρ_0 is the path loss of the LOS link.
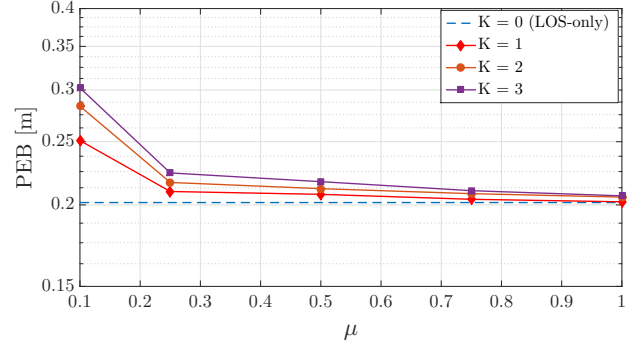

Fig. 2: PEB on the estimation of $\boldsymbol{p}$ as a function of the degree of separation among LOS and NLOS paths μ, for a varying number of NLOS paths.

B. Results and Discussion

1) Analysis of the theoretical bounds: we start the analysis by providing a numerical interpretation of the relevant CRLBs derived using the FIM analysis in Sec. III. In Fig. 2, we investigate the achievable theoretical accuracy in the estimation of the desired MS position $\boldsymbol{p}$ in presence of a number of NLOS paths K varying from a minimum of zero (i.e., LOS-only scenario) up to a maximum of three [50]. To reproduce different geometric configurations of the environment, we fix three reference directions from the MS to the scatterers to $-20°$, $50°$ and $70°$, respectively, and vary each position $\boldsymbol{s}_k$ ($k \geq 1$) along its corresponding direction in order to obtain a distance between the MS and the k-th scatterer equal to $d_{k,2} = \ell_k \mu$, with $\mu \in (0, 1]$ a scaling parameter introduced to increase or decrease the degree of separation (in terms of both TOF and AOD) among the LOS path and the NLOS paths. The three reference distances are set to $\ell_1 = 20$ m, $\ell_2 = 28$ m, and $\ell_3 = 36$ m, so that the resulting scenario is compatible with the expected coverage in mmWave 5G systems [13]. In agreement with the theoretical findings in Sec. III-D, we observe that the PEB does not experience significant changes as K increases, confirming that the estimation of $\boldsymbol{p}$ is not harmed by the presence of the additional NLOS paths at the receive side. This behavior also confirms the orthogonality among the different paths, since the NLOS paths start to have a noticeable effect only for very small values of μ. Furthermore, the very slight differences among the PEB curves reveal that the residual reciprocal interference among the paths is mainly linked to the overall multipath power and it is otherwise independent from the effective number of NLOS paths K. Therefore, to ease the presentation and without loss of generality, in the following we stick to the case of a single NLOS path (i.e., $K = 1$) and evaluate the proposed algorithm performance for different values of the multipath power. Finally, notice that the values assumed by the PEB demonstrate that cm-level localization accuracy can be achieved in the considered mmWave MISO setup, in spite of the fact that the receiver can only exploit a single antenna to cope with multipath propagation.

2) Comparison between channel domain and position domain estimation: the approach proposed in Sec. IV-A originates from the idea that a first initial estimate of the unknown vector $\boldsymbol{\Theta}$ can be obtained by searching for the $K+1$ dominant
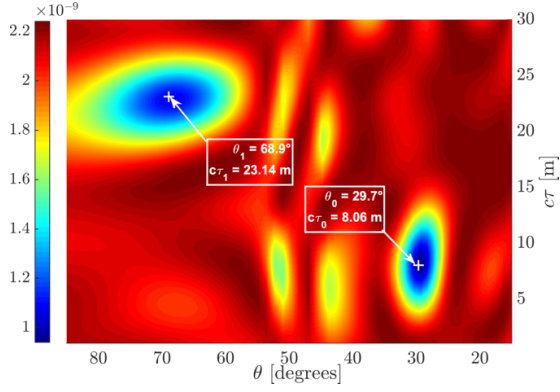
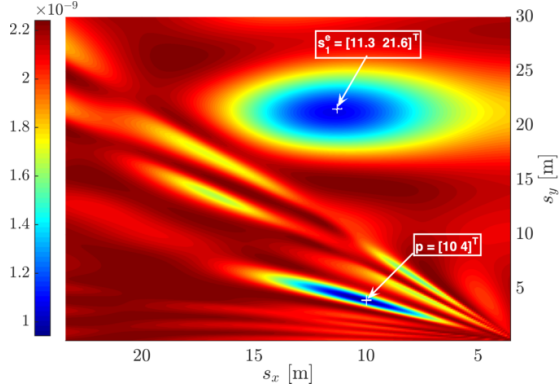Fig. 3: Possible evaluation of the cost function $L_0(\theta, \tau)$ for a scenario with $K = 1$ NLOS path.

Fig. 4: Possible evaluation of the cost function $L_0(\boldsymbol{s})$ for a scenario with $K = 1$ NLOS path.

(a) RMSE on the estimation of d_k.

(b) RMSE on the estimation of θ_k.

Fig. 5: RMSEs on $d_k = c\tau_k$ and θ_k estimation in comparison with the CRLBs as a function of the SNR, for a LMR = 5 dB.

minima in the single-path cost function $L_0(\theta, \tau)$. To validate such an intuition, in Fig. 3 we report a graphical example of a possible evaluation of $L_0(\theta, \tau)$ over a discrete two-dimensional 64×64 grid [1] of (θ, τ) pairs. The simulation is conducted assuming a single scatterer placed at $\boldsymbol{s}_1 = [8\ 13]^{\mathrm{T}}$ m, which generates a reflected NLOS path having a power 3 dB less than the LOS, at SNR = 5 dB. As expected, the cost function is highly non-linear and exhibits several local minima. However, the two dominant minima are in the neighborhood of the actual (θ_k, τ_k) pairs, $k = 0, 1$ (indicated by crosses), meaning that $L_0(\theta, \tau)$ is able to capture the angular and time "signature" of each individual path, although with an accuracy that worsens for lower SNR and less separable paths. This is remarkable since $L_0(\theta, \tau)$ is a suboptimal function that ignores the presence of more than one path in the received signal $\boldsymbol{Y}$.

For the sake of comparison, in Fig. 4 we report the evaluation of the position-domain cost function $L_0(\boldsymbol{s})$ (see Sec. IV-D) over a discrete grid of (s_x, s_y) pairs obtained from the previous 64×64 grid (in the channel domain) by applying a Cartesian transformation to each (θ, τ) pair (i.e., $[s_x\ s_y]^{\mathrm{T}} = c\tau[\cos\ \theta \sin\theta]^{\mathrm{T}}$ pair), while the remaining parameters are set as in Fig. 3. We observe that, also in the location domain, there are two dominant minima that clearly

[1] Notice that we are considering a fine grid (with resolution 0.2 m in range and 0.5 degrees in angle) only for the sake of visualization; for practical implementation, a very coarse grid (with resolution 2 m in range and 4 degrees in angle) is sufficient to achieve best performance.
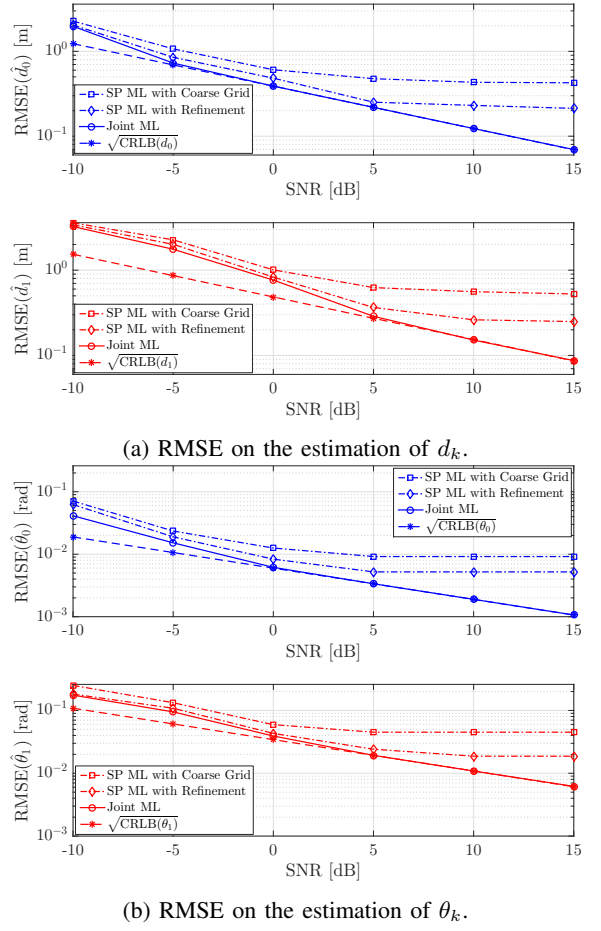
emerge in evaluating the cost function $L_0(\boldsymbol{s})$. In line with the discussion in Sec. IV-D, the bottom-most minimum occurs in the neighborhood of the actual MS position $\boldsymbol{p}$, while the other one (linked to the NLOS parameters) is located in the vicinity of the equivalent scatterer position $\boldsymbol{s}_1^e = [11.3\ 21.6]^{\mathrm{T}}$ m.[2]

3) Performance assessment for LOS stronger than NLOS: we start the performance assessment by considering the more typical case in which the LOS path is received with a power greater than the NLOS, that is, we assume the presence of a single scatterer at $\boldsymbol{s}_1 = [8\ 13]^{\mathrm{T}}$ m which produces a LMR = 5 dB. Fig. 5 reports the RMSEs on the estimation of the channel parameters d_k and θ_k, $k = 0, 1$, as a function of the SNR. The proposed estimator is labeled as "Joint ML" and it is implemented in two-steps: in the first one, an initial estimate of $\boldsymbol{\Theta}$ is obtained by searching for the $K + 1$ dominant minima

[2] It is worth noting that a naive search of the first $K + 1$ minima in any single-path cost function would likely produce erroneous estimates of the sought channel or position parameters, respectively: in fact, since each dominant minimum is quite spread (blue areas in both figures), the search would likely lead to incorrectly selecting multiple local minima belonging to the neighborhood of the same dominant minimum. To overcome such a drawback, one can resort to the well-known space-alternating generalized expectation-maximization (SAGE) method, which sequentially estimate each (θ_k, τ_k) pair and compensate its contribution before searching for the next dominant minimum (i.e., the next (θ_k, τ_k) pair) in the cost function. This approach, theoretically introduced in [51], has been extensively applied for parameter extraction from extensive channel measurement data [52], [53].

in $L_0(\theta, \tau)$ over a coarse 8×8 grid built from pairs (θ_k, τ_k); the estimated vector $\hat{\Theta}$ is then used to initialize a Nelder-Mead procedure which iteratively solves the $(K + 1)$-dimensional ML estimation problem in (29). For the sake of comparison, we also report the performance of the algorithms that approach the estimation problem by assuming a simplified single-path (SP) model. More precisely, we label as "SP ML with Coarse Grid" the algorithm that simply optimizes $L_0(\theta, \tau)$ over the coarse 8×8 grid to estimate Θ (i.e., the first step of the proposed Joint ML approach). The SP estimation performance can be further improved by using each estimated $(\hat{\theta}_k, \hat{\tau}_k)$ pair in $\hat{\Theta}$ to initialize a Nelder-Mead procedure that numerically optimize the SP cost function $L_0(\theta, \tau)$, yielding a refined estimate of Θ; in the following, we label such an approach as "SP ML with Refinement". Notice that the optimization in the second step of both the "SP ML with Refinement" and the proposed "Joint ML" can be efficiently performed in a relatively short time, with the latter requiring only a slightly increased runtime compared to the former due to the larger size of the vectors involved in the iterative optimization. As concerns the theoretical lower bounds, each $\sqrt{\mathrm{CRLB}(\cdot)}$ is obtained by inverting the FIM in either channel (ref. eq. (6)) or location (ref. eq. (13)) domain, selecting the corresponding diagonal entries and taking the square root.

By comparing the RMSEs in Fig. 5, we observe that the LOS channel parameters are estimated more accurately than the NLOS ones (as also reflected in the corresponding bounds), due to the stronger power of the former compared to latter. The "SP ML with Coarse Grid" algorithm (dash-dot curves with square markers) provides satisfactory initial estimates of both AODs and TOFs parameters, with an accuracy that increases with the SNR (since the powers of the LOS and NLOS paths increase accordingly) and with a reduced complexity thanks to the coarse grid used in the estimation process. Although the performance further improves when a subsequent iterative 2D refinement is applied (see dash-dot curves with diamond markers), both the SP algorithms are still unable to achieve the theoretical lower bounds, as confirmed by the position errors reported in Fig. 6. The existing gap clearly demonstrates that the algorithms derived assuming a simplified SP model cannot effectively cope with the residual mutual interference among the received paths. On the other hand, the solid curves show that the proposed Joint ML estimator offers the best performance: indeed, the RMSE of $\hat{p}$ approaches the bound already for SNR = -5 dB, while the mapping of the scatterer position becomes increasingly more accurate until reaching the bound for SNR = 5 dB.

4) Performance assessment for LOS weaker than NLOS: to challenge the proposed Joint ML estimator, we consider the case in which the power of the NLOS path is 5 dB higher than that of the LOS, that is, we set LMR = -5 dB. This setup is representative of scenarios in which the LOS path is severely attenuated. The RMSEs of $\hat{p}$ and $\hat{s}_1$ are reported in Fig. 7: in this case, the higher power in the NLOS path translates into more advantageous conditions for mapping the scatterer position, which in fact is more accurately estimated compared to the MS position, as confirmed by the smaller values of the bounds (dashed curves). As it can be observed, in this case the
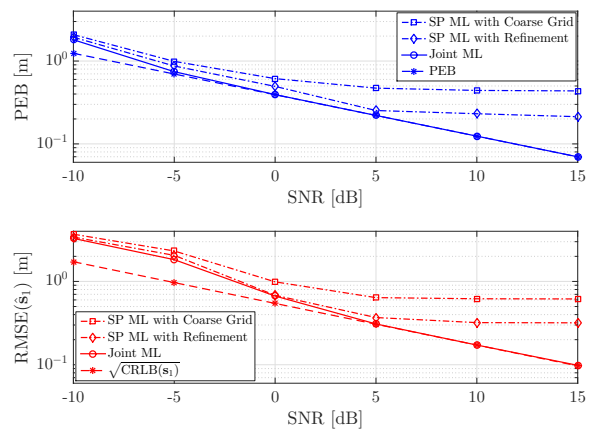

Fig. 6: RMSEs on MS and scatterer position estimation versus CRLBs as a function of the SNR, for LMR = 5 dB.
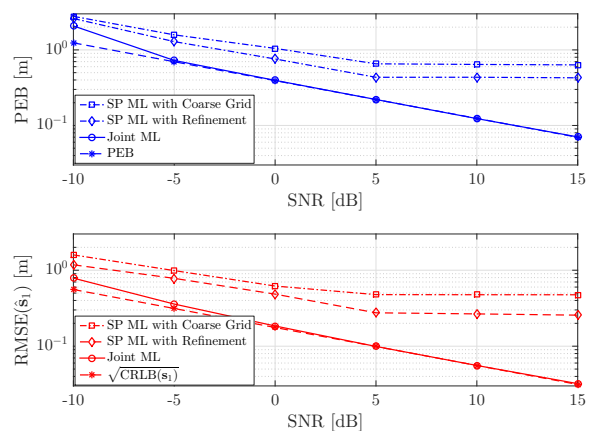

Fig. 7: RMSEs on MS and scatterer position estimation versus CRLBs as a function of the SNR, for LMR = -5 dB.

performances of the SP algorithms significantly deviate from the theoretical bounds. Remarkably, the proposed Joint ML estimator performs well even when the LOS path is highly attenuated, providing a very accurate localization of the MS and mapping of the scatterer already at about 0 dB SNR.

To further challenge the algorithms, we investigate the case in which the LOS and NLOS paths are not easily separable in both space and time domains, i.e., they are non-orthogonal according to the definition given in Sec. III-A. More precisely, we moved the position of the scatterer closer to the MS position, that is, we set $s_1 = \begin{bmatrix} 11 & 16 \end{bmatrix}^{\mathsf{T}}$ m. In this case, $\theta_0 = 69°$ and $\theta_1 = 63°$, while the corresponding TOFs are such that $c\tau_0 = 14$ m and $c\tau_1 = 22$ m. This scenario is quite challenging being the angular and delay separation between the paths drastically close to the minimum spatial and time resolution of the system for the considered values of the parameters (i.e., $2/N \approx 6°$ resolution in angle and $c/B = 7.5$ m resolution in distance). The obtained results are reported in Fig. 8. Interestingly, despite the more challenging scenario (as confirmed by the higher values of the CRLBs), the proposed approach can correctly cope also with the presence of NLOS paths that are very close (in both time and space) to the LOS link, with a slight performance degradation only for small values of the SNR.
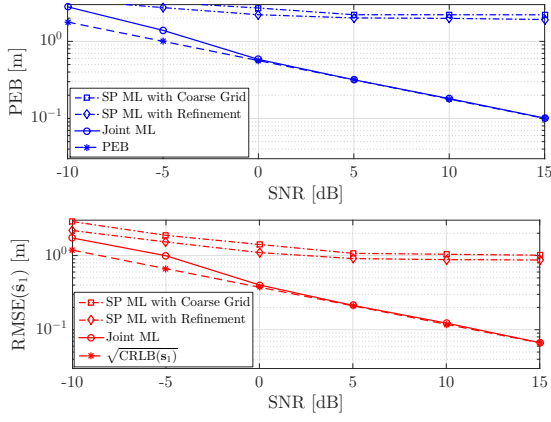
Fig. 8: RMSEs on MS and scatterer position estimation versus CRLBs as a function of the SNR, for LMR $= -5$ dB and non-orthogonal LOS and NLOS paths.

Fig. 9: RMSEs on MS and scatterer position estimation versus CRLBs as a function of the LMR, for SNR $= 10$ dB.

5) Performance assessment as a function of the multipath power: to corroborate the above results, we further analyze the algorithms behavior assuming a fixed value of the SNR and varying the multipath power in terms of LMR between -10 dB and 10 dB, so as to obtain performance representative of a number of different operational conditions. In Fig. 9, we show the RMSEs on the estimation of $\boldsymbol{p}$ and $\boldsymbol{s}_1$ as a function of the LMR, for a SNR $= 10$ dB. In agreement with the theoretical findings in Sec. III-D as well as with the analysis reported in Fig. 2, the PEB remains practically constant as the LMR changes, thus confirming the very weak dependency of LOS on the NLOS path, that is, the estimation of $\boldsymbol{p}$ is not harmed by the presence of multipath propagation. On the other hand, the dashed (red) curve shows that the accuracy achievable in the estimation of $\boldsymbol{s}_1$ progressively worsens as the power of the multipath diminishes. As it can be noticed, the performances of the SP algorithms are in trade-off: indeed, the RMSEs on the estimation of $\boldsymbol{p}$ tend to decrease as the LMR increases; conversely, the RMSEs of $\hat{\boldsymbol{s}}_1$ experiences an evident increase as the power of the NLOS path drops. Again, this behavior confirms that the performances are better for the more powerful path. Interestingly, the proposed Joint ML approach, thanks to its optimality, is able to cope with the less accurate scatterer position estimate for high LMRs, and vice versa with the less accurate MS position estimate for low LMRs. Indeed, the solid curves show that the joint estimator enables a satisfactory localization and mapping in all the different operating conditions, significantly outperforming the SP competitors and attaining the bounds for even moderate values of the SNR.

As a final remark, notice that all the performances above are very good despite the quite moderate values of the system parameters. Realistic values are more favorable, e.g. the number of transmit antennas N_{BS} is typically larger, hence the resulting performance monotonically improves (figures not reported due to lack of space).

VI. CONCLUSION

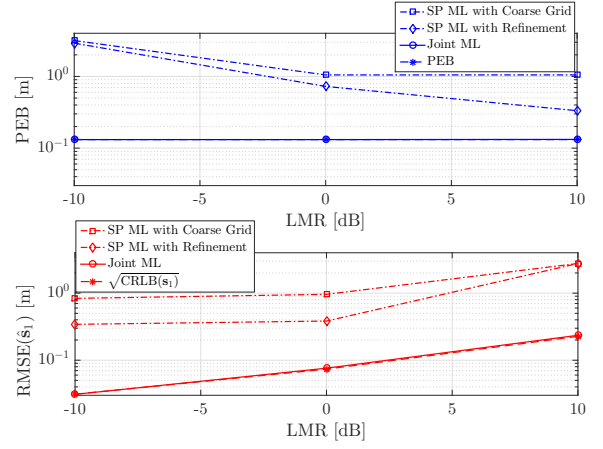The problem of single-snapshot estimation of the unknown MS position and mapping of scatterers locations in a mmWave MISO system has been addressed. The localization process is based on the combined use of AOD and TOF information, which can be estimated from a single pilot signal broadcast in DL by a BS. The Fisher information analysis demonstrated that localization and mapping is still possible also when using a single-antenna receiver but, differently from the MIMO setup, NLOS information cannot be used to improve the estimation of the MS position. We formulated the joint ML estimation problem in the channel domain and proposed and evaluated a low-complexity initialization method, which has an equivalent formulation in the position domain.

APPENDIX A
DERIVATION OF FIM ELEMENTS IN (7)

In the following, we provide the exact expressions of the entries of the FIM matrix in (7), derived based on (8). We introduce $\kappa_n = 2\pi n/(N T_S)$, $\beta_{h,\ell} = \frac{2 N_{\text{BS}}}{\sigma^2} \alpha_h^* \alpha_\ell \exp(j\kappa_n(\tau_h - \tau_\ell))$ and $\boldsymbol{A}_{h,\ell} = \boldsymbol{a}_{\text{BS}}(\theta_h)\boldsymbol{a}_{\text{BS}}^{\text{H}}(\theta_\ell)$. We start from the elements linked to the parameters θ_k and τ_k, which are given by

$$\Lambda(\tau_h, \tau_\ell) = \sum_{g,n} \Re\left\{\beta_{h,\ell}\kappa_n^2 (\boldsymbol{z}^g[n])^{\text{H}} \boldsymbol{A}_{h,\ell} \boldsymbol{z}^g[n]\right\},$$

$$\Lambda(\theta_h, \theta_\ell) = \sum_{g,n} \Re\left\{\beta_{h,\ell}(\boldsymbol{z}^g[n])^{\text{H}} \boldsymbol{D}_h^{\text{H}} \boldsymbol{A}_{h,\ell} \boldsymbol{D}_\ell \boldsymbol{z}^g[n]\right\},$$

$$\Lambda(\tau_h, \theta_\ell) = \sum_{g,n} \Re\left\{j\kappa_n\beta_{h,\ell}(\boldsymbol{z}^g[n])^H \boldsymbol{A}_{h,\ell} \boldsymbol{D}_\ell \boldsymbol{z}^g[n]\right\},$$

where the matrix $\boldsymbol{D}_u$ with subscript u replaced by either h or ℓ is given by

$$\boldsymbol{D}_u = -j\frac{2\pi}{\lambda_c} d \cos\theta_u \text{diag}[0 \ 1 \ \cdots \ (N_{\text{BS}} - 1)]$$

with $\text{diag}(\cdot)$ a function which constructs a diagonal matrix with its entries.

The elements including the channel amplitudes r_k and phases ϕ_k are obtained as

$$\Lambda(\tau_h, r_\ell) = \sum_{g,n} \Re\{j\text{e}^{j\phi_\ell} \frac{\beta_{h,\ell}}{\alpha_\ell} \kappa_n (\boldsymbol{z}^g[n])^H \boldsymbol{A}_{h,\ell} \boldsymbol{z}^g[n]\},$$

$$\Lambda(\tau_h, \phi_\ell) = \sum_{g,n} \Re\{-\beta_{h,\ell}\kappa_n (\boldsymbol{z}^g[n])^H \boldsymbol{A}_{h,\ell} \boldsymbol{z}^g[n]\},$$

$$\Lambda(\theta_h, r_\ell) = \sum_{g,n} \Re\{j\mathrm{e}^{j\phi_\ell}\frac{\beta_{h,\ell}}{\alpha_\ell}(\boldsymbol{z}^g[n])^H \boldsymbol{D}_h^H \boldsymbol{A}_{h,\ell}\boldsymbol{z}^g[n]\},$$

$$\Lambda(\theta_h, \phi_\ell) = \sum_{g,n} \Re\{j\beta_{h,\ell}(\boldsymbol{z}^g[n])^H \boldsymbol{D}_h^H \boldsymbol{A}_{h,\ell}\boldsymbol{z}^g[n]\},$$

$$\Lambda(r_h, r_\ell) = \sum_{g,n} \Re\{\frac{\beta_{h,\ell}}{\alpha_h^*\alpha_\ell}\mathrm{e}^{j(\phi_\ell-\phi_h)}(\boldsymbol{z}^g[n])^H \boldsymbol{A}_{h,\ell}\boldsymbol{z}^g[n]\},$$

$$\Lambda(\phi_h, \phi_\ell) = \sum_{g,n} \Re\{\beta_{h,\ell}(\boldsymbol{z}^g[n])^H \boldsymbol{A}_{h,\ell}\boldsymbol{z}^g[n]\},$$

$$\Lambda(r_h, \phi_\ell) = \sum_{g,n} \Re\{j\frac{\beta_{h,\ell}}{\alpha_h^*}\mathrm{e}^{-j\phi_h}(\boldsymbol{z}^g[n])^H \boldsymbol{A}_{h,\ell}\boldsymbol{z}^g[n]\}.$$

ACKNOWLEDGMENTS

REFERENCES

[1] T. S. Rappaport, S. Sun, R. Mayzus, H. Zhao, Y. Azar, K. Wang, G. N. Wong, J. K. Schulz, M. Samimi, and F. Gutierrez, "Millimeter wave mobile communications for 5G cellular: It will work!," *IEEE Access*, vol. 1, pp. 335–349, 2013.

[2] K. Witrisal, P. Meissner, E. Leitinger, Y. Shen, C. Gustafson, F. Tufvesson, K. Haneda, D. Dardari, A. F. Molisch, A. Conti, and M. Z. Win, "High-accuracy localization for assisted living: 5G systems will turn multipath channels from foe to friend," *IEEE Sig. Proc. Magazine*, vol. 33, no. 2, pp. 59–70, 2016.

[3] L. Lu, G. Y. Li, A. L. Swindlehurst, A. Ashikhmin, and R. Zhang, "An overview of massive MIMO: Benefits and Challenges," *IEEE Journal of Selected Topics in Signal Proc.*, vol. 8, no. 5, pp. 742–758, 2014.

[4] T. Bai and R. W. Heath, "Coverage and rate analysis for millimeter-wave cellular networks," *IEEE Trans. on Wireless Comm.*, vol. 14, no. 2, pp. 1100–1114, 2015.

[5] E. G. Larsson, O. Edfors, F. Tufvesson, and T. L. Marzetta, "Massive MIMO for next generation wireless systems," *IEEE Comm. Magazine*, vol. 52, no. 2, pp. 186–195, 2014.

[6] H. Wymeersch, G. Seco-Granados, G. Destino, D. Dardari, and F. Tufvesson, "5G mmWave positioning for vehicular networks," *IEEE Wireless Comm.*, vol. 24, no. 6, pp. 80–86, 2017.

[7] J. A. del Peral-Rosado, R. Raulefs, J. A. Lopez-Salcedo, and G. Seco-Granados, "Survey of cellular mobile radio localization methods: From 1G to 5G," *IEEE Comm. Surveys Tutorials*, vol. 20, no. 2, pp. 1124–1148, 2018.

[8] A. Kakkavas, M. H. Castañeda García, R. A. Stirling-Gallacher, and J. A. Nossek, "Performance limits of single-anchor millimeter-wave positioning," *IEEE Trans. on Wireless Comm.*, vol. 18, no. 11, pp. 5196–5210, 2019.

[9] Z. Abu-Shaban, X. Zhou, T. Abhayapala, G. Seco-Granados, and H. Wymeersch, "Error bounds for uplink and downlink 3D localization in 5G millimeter wave systems," *IEEE Trans. on Wireless Comm.*, vol. 17, no. 8, pp. 4939–4954, 2018.

[10] A. Shahmansoori, G. E. Garcia, G. Destino, G. Seco-Granados, and H. Wymeersch, "Position and orientation estimation through millimeter-wave MIMO in 5G systems," *IEEE Trans. on Wireless Comm.*, vol. 17, no. 3, pp. 1822–1835, 2018.

[11] N. Garcia, H. Wymeersch, E. G. Larsson, A. M. Haimovich, and M. Coulon, "Direct localization for massive MIMO," *IEEE Trans. on Signal Proc.*, vol. 65, no. 10, pp. 2475–2487, 2017.

[12] A. Hu, T. Lv, H. Gao, Z. Zhang, and S. Yang, "An ESPRIT-based approach for 2-D localization of incoherently distributed sources in massive MIMO systems," *IEEE Journal of Selected Topics in Signal Proc.*, vol. 8, no. 5, pp. 996–1011, 2014.

[13] M. Koivisto, M. Costa, J. Werner, K. Heiska, J. Talvitie, K. Leppnen, V. Koivunen, and M. Valkama, "Joint device positioning and clock synchronization in 5G ultra-dense networks," *IEEE Trans. on Wireless Comm.*, vol. 16, no. 5, pp. 2866–2881, 2017.

[14] J. Palacios, G. Bielsa, P. Casari, and J. Widmer, "Single- and multiple-access point indoor localization for millimeter-wave networks," *IEEE Trans. on Wireless Comm.*, vol. 18, no. 3, pp. 1927–1942, 2019.

[15] R. Mendrzik, H. Wymeersch, G. Bauch, and Z. Abu-Shaban, "Harnessing NLOS components for position and orientation estimation in 5G millimeter wave MIMO," *IEEE Trans. on Wireless Comm.*, vol. 18, no. 1, pp. 93–107, 2019.

[16] H. Durrant-Whyte and T. Bailey, "Simultaneous localization and mapping: part I," *IEEE Robotics & Automation Magazine*, vol. 13, no. 2, pp. 99–110, 2006.

[17] T. Bailey and H. Durrant-Whyte, "Simultaneous localization and mapping (SLAM): part II," *IEEE Robotics & Automation Magazine*, vol. 13, no. 3, pp. 108–117, 2006.

[18] J. Talvitie, M. Valkama, G. Destino, and H. Wymeersch, "Novel algorithms for high-accuracy joint position and orientation estimation in 5G mmWave systems," in *2017 IEEE Globecom Workshops (GC Wkshps)*, 2017, pp. 1–7.

[19] R. Mendrzik, H. Wymeersch, and G. Bauch, "Joint localization and mapping through millimeter wave MIMO in 5G systems," in *2018 IEEE Global Comm. Conference (GLOBECOM)*, 2018, pp. 1–6.

[20] H. Kim, K. Granström, L. Gao, G. Battistelli, S. Kim, and H. Wymeersch, "5G mmwave cooperative positioning and mapping using multi-model PHD filter and map fusion," *IEEE Trans. on Wireless Comm.*, vol. 19, no. 6, pp. 3782–3795, 2020.

[21] X. Li, E. Leitinger, M. Oskarsson, K. Åström, and F. Tufvesson, "Massive MIMO-based localization and mapping exploiting phase information of multipath components," *IEEE Trans. on Wireless Comm.*, vol. 18, no. 9, pp. 4254–4267, 2019.

[22] E. Westberg, J. Staudinger, J. Annes, and V. Shilimkar, "5G infrastructure RF solutions: Challenges and opportunities," *IEEE Microwave Magazine*, vol. 20, no. 12, pp. 51–58, 2019.

[23] C. Gentner, T. Jost, W. Wang, S. Zhang, A. Dammann, and U. Fiebig, "Multipath assisted positioning with simultaneous localization and mapping," *IEEE Trans. on Wireless Comm.*, vol. 15, no. 9, pp. 6104–6117, 2016.

[24] E. Leitinger, F. Meyer, F. Hlawatsch, K. Witrisal, F. Tufvesson, and M. Z. Win, "A belief propagation algorithm for multipath-based SLAM," *IEEE Trans. on Wireless Comm.*, vol. 18, no. 12, pp. 5613–5629, 2019.

[25] C. Huang, A. Zappone, G. C. Alexandropoulos, M. Debbah, and C. Yuen, "Reconfigurable intelligent surfaces for energy efficiency in wireless communication," *IEEE Trans. on Wireless Comm.*, vol. 18, no. 8, pp. 4157–4170, 2019.

[26] C. Huang, R. Mo, and Y. Yuen, "Reconfigurable intelligent surface assisted multiuser MISO systems exploiting deep reinforcement learning," *IEEE Journal on Selected Areas in Comm.*, vol. 38, no. 8, pp. 1839–1850, 2020.

[27] A. Fascista, A. Coluccia, H. Wymeersch, and G. Seco-Granados, "RIS-aided Joint Localization and Synchronization with a Single-Antenna MmWave Receiver," *arXiv e-prints*, p. arXiv:2010.14825, Oct. 2020.

[28] A. Fascista, A. Coluccia, H. Wymeersch, and G. Seco-Granados, "Low-complexity accurate mmwave positioning for single-antenna users based on angle-of-departure and adaptive beamforming," in *IEEE Intern. Conf. on Acoustics, Speech and Signal Proc. (ICASSP)*, 2020, pp. 4866–4870.

[29] A. Fascista, A. Coluccia, H. Wymeersch, and G. Seco-Granados, "Millimeter-wave downlink positioning with a single-antenna receiver," *IEEE Trans. on Wireless Comm.*, vol. 18, no. 9, pp. 4479–4490, 2019.

[30] A. Alkhateeb, J. Mo, N. Gonzalez-Prelcic, and R. W. Heath, "MIMO precoding and combining solutions for millimeter-wave systems," *IEEE Comm. Magazine*, vol. 52, no. 12, pp. 122–131, 2014.

[31] C. Huang, L. Liu, C. Yuen, and S. Sun, "Iterative channel estimation using LSE and sparse message passing for mmwave MIMO systems," *IEEE Trans. on Signal Proc.*, vol. 67, no. 1, pp. 245–259, 2019 .

[32] A. Alkhateeb and R. W. Heath, "Frequency selective hybrid precoding for limited feedback millimeter wave systems," *IEEE Trans. on Comm.*, vol. 64, no. 5, pp. 1801–1818, 2016.

[33] J. Brady, N. Behdad, and A. M. Sayeed, "Beamspace MIMO for millimeter-wave communications: System architecture, modeling, analysis, and measurements," *IEEE Trans. on Ant. and Prop.*, vol. 61, no. 7, pp. 3814–3827, 2013.

[34] J. H. Brady and A. M. Sayeed, "Wideband communication with high-dimensional arrays: New results and transceiver architectures," in *IEEE Intern. Conf. on Comm. Workshop (ICCW)*, 2015, pp. 1042–1047.

[35] Z. Abu-Shaban, H. Wymeersch, T. Abhayapala, and G. Seco-Granados, "Single-anchor two-way localization bounds for 5G mmwave systems," *IEEE Trans. on Vehic. Tech.*, pp. 1–1, 2020.

[36] V. Sark, E. Grass, and J. Gutirrez, "Multi-way ranging with clock offset compensation," in *Advances in Wireless and Optical Communications (RTUWO)*, 2015, pp. 68–71.

[37] S. Kay, *Fundamentals of Statistical Signal Processing: Estimation Theory*, Prentice-Hall, Inc., USA, 1993.

[38] Y. Shen and M. Z. Win, "Fundamental limits of wideband localization part I: A general framework," *IEEE Trans. on Inf. Theory*, vol. 56, no. 10, pp. 4956–4980, 2010.

[39] D. R. Cox and N. Reid, "Parameter orthogonality and approximate conditional inference," *Journal of the Royal Statistical Society: Series B (Methodological)*, vol. 49, no. 1, pp. 1–18, 1987.

[40] E. Leitinger, P. Meissner, C. Rdisser, G. Dumphart, and K. Witrisal, "Evaluation of position-related information in multipath components for indoor positioning," *IEEE Journal on Selected Areas in Comm.*, vol. 33, no. 11, pp. 2313–2328, 2015.

[41] H. Wymeersch, N. Garcia, H. Kim, G. Seco-Granados, S. Kim, F. Wen, and M. Fröhle, "5G mmwave downlink vehicular positioning," in *2018 IEEE Global Comm. Conf. (GLOBECOM)*, 2018, pp. 206–212.

[42] C. N. Barati, S. A. Hosseini, M. Mezzavilla, T. Korakis, S. S. Panwar, S. Rangan, and M. Zorzi, "Initial access in millimeter wave cellular systems," *IEEE Trans. on Wireless Comm.*, vol. 15, no. 12, pp. 7926–7940, 2016.

[43] M. Giordani, M. Mezzavilla, and M. Zorzi, "Initial access in 5G mmWave cellular networks," *IEEE Comm. Magazine*, vol. 54, no. 11, pp. 40–47, 2016.

[44] William H. Press, Saul A. Teukolsky, William T. Vetterling, and Brian P. Flannery, *Numerical Recipes 3rd Edition: The Art of Scientific Computing*, Cambridge University Press, USA, 3 edition, 2007.

[45] Jeffrey C. Lagarias, James A. Reeds, Margaret H. Wright, and Paul E. Wright, "Convergence properties of the nelder–mead simplex method in low dimensions," *SIAM J. on Optimization*, vol. 9, no. 1, pp. 112–147, May 1998.

[46] J. Khodjaev, Y. Park, and A. Saeed Malik, "Survey of NLOS identification and error mitigation problems in UWB-based positioning algorithms for dense environments," *Annals of Telecommunications*, vol. 65, no. 1, pp. 301–311, 2009.

[47] L. Cong and W. Zhuang, "Nonline-of-sight error mitigation in mobile location," *IEEE Trans. on Wireless Comm.*, vol. 4, no. 2, pp. 560–573, 2005.

[48] Q. C. Li, G. Wu, and T. S. Rappaport, "Channel model for millimeter-wave communications based on geometry statistics," in *IEEE Globecom Workshops (GC Wkshps)*, 2014, pp. 427–432.

[49] Q. Li, H. Shirani-Mehr, T. Balercia, A. Papathanassiou, G. Wu, S. Sun, M. K. Samimi, and T. S. Rappaport, "Validation of a geometry-based statistical mmwave channel model using ray-tracing simulation," in *IEEE Vehic. Tech. Conf. (VTC Spring)*, 2015, pp. 1–5.

[50] T. S. Rappaport, Y. Xing, G. R. MacCartney, A. F. Molisch, E. Mellios, and J. Zhang, "Overview of millimeter wave communications for fifth-generation (5G) wireless networkswith a focus on propagation models," *IEEE Trans. on Ant. and Prop.*, vol. 65, no. 12, pp. 6213–6230, 2017.

[51] J. A. Fessler and A. O. Hero, "Space-alternating generalized expectation-maximization algorithm," *IEEE Trans. on Signal Proc.*, vol. 42, no. 10, pp. 2664–2677, 1994.

[52] B. H. Fleury, M. Tschudin, R. Heddergott, D. Dahlhaus, and K. Ingeman Pedersen, "Channel parameter estimation in mobile radio environments using the SAGE algorithm," *IEEE Journal on Selected Areas in Comm.*, vol. 17, no. 3, pp. 434–450, 1999.

[53] A. Pin, R. Rinaldo, A. Tonello, C. Marshall, M. Driusso, A. Biason, and A. D. Torre, "LTE ranging measurement using uplink opportunistic signals and the SAGE algorithm," in *27th European Signal Proc. Conf. (EUSIPCO)*, 2019, pp. 1–5.

Angelo Coluccia (M'13 - SM'16) received the Ph.D. degree in Information Engineering in 2011 and is currently an Associate Professor of Telecommunications at the Department of Engineering, University of Salento (Lecce, Italy). He has been a research fellow at Forschungszentrum Telekommunikation Wien (Vienna, Austria), and has held a visiting position at the Department of Electronics, Optronics, and Signals of the Institut Supérieur de l' Aéronautique et de l'Espace (ISAE-Supaero, Toulouse, France). His research interests are in the area of multi-channel, multi-sensor, and multi-agent statistical signal processing for detection, estimation, localization, and learning problems. Relevant application fields are radar, wireless networks (including 5G and beyond), and emerging network contexts (including intelligent cyber-physical systems, smart devices, and social networks). He is Senior Member of IEEE and Member of the Technical Area Committee in Signal Processing for Multisensor Systems of EURASIP.

Henk Wymeersch (M'05 - SM'19) obtained the Ph.D. degree in Electrical Engineering/Applied Sciences in 2005 from Ghent University, Belgium. He is currently a Professor of Communication Systems with the Department of Electrical Engineering at Chalmers University of Technology, Sweden. He is also a Distinguished Research Associate with Eindhoven University of Technology. Prior to joining Chalmers, he was a postdoctoral researcher from 2005 until 2009 with the Laboratory for Information and Decision Systems at the Massachusetts Institute of Technology. Prof. Wymeersch served as Associate Editor for IEEE Communication Letters (2009-2013), IEEE Transactions on Wireless Communications (since 2013), and IEEE Transactions on Communications (2016-2018). During 2019-2021, he is a IEEE Distinguished Lecturer with the Vehicular Technology Society. His current research interests include the convergence of communication and sensing, in a 5G and Beyond 5G context.

Gonzalo Seco-Granados (M'02 - SM'08) received the Ph.D. degree in telecommunications engineering from the Universitat Politecnica de Catalunya, Spain, in 2000, and the M.B.A. degree from the IESE Business School, Spain, in 2002. From 2002 to 2005, he was a member of the European Space Agency, where he was involved in the design of the Galileo system and receivers. In 2015 and 2019, he was a Fulbright Visiting Scholar at the University of California, Irvine, USA. He is currently Professor in the Dept. of Telecommunication, Universitat Autonoma de Barcelona, where he has served as Vice Dean of the Engineering School during 2011-2019. His research interests include statistical signal processing with application to GNSS and 5G localization. Since 2018, he has been serving as a member of the Sensor Array and Multichannel Technical Committee for the IEEE Signal Processing Society. Since 2019, he is President of the Spanish Chapter of the IEEE Aerospace and Electronic Systems Society.

Alessio Fascista (M'19) received the Ph.D. degree in Engineering of Complex Systems from the University of Salento (Lecce, Italy) in 2019. He is currently an Assistant Professor of Telecommunications at the Department of Innovation Engineering, University of Salento. In 2018, he was a visiting PhD with the Signal Processing for Communications & Navigation (SPCOMNAV) group, Department of Telecommunications and Systems Engineering, Universitat Autònoma de Barcelona (UAB), Spain. His main research interests are in the field of telecommunications with focus on statistical signal processing for detection, estimation, and localization in terrestrial wireless systems.